U.S. DEPARTMENT OF COMMERCE
NATIONAL OCEANIC AND ATMOSPHERIC ADMINISTRATION
NATIONAL WEATHER SERVICE
SYSTEMS DEVELOPMENT OFFICE
TECHNIQUES DEVELOPMENT LABORATORY

TDL OFFICE NOTE 81-9

SIX-TO-TWELVE HOUR FORECASTING OF METEOROLOGICAL FIELDS USING A PATTERN CORRELATION MODEL

Jerome P. Charba, Paul A. Jendrowski,
and George W. VandenBerghe

December 1981

SIX-TO-TWELVE HOUR FORECASTING OF METEOROLOGICAL FIELDS USING A PATTERN CORRELATION MODEL

Jerome P. Charba, Paul A. Jendrowski, and George W. VandenBerghe

1. INTRODUCTION

This note describes a simple model that uses a pattern correlation technique to produce short range forecasts (12 hours or less) of various meteorological fields with high spatial resolution. The forecasts are intended for use as input to statistical prediction models and possibly as an aid in subjective forecasting by field forecasters. The model, adapted from Clodman (1980), produces a forecast in two steps. First, the expected large scale translation and development fields of the meteorological variable of interest are extracted from two guidance fields, which are separated in time. The translation and growth fields are then applied to a current high spatial resolution analysis of the variable to obtain the desired detailed forecast.

The two guidance fields may be obtained from large scale analyses of the variable (or another quite similar variable), one valid at the current time and the other valid 6-12 h earlier. Alternatively, the guidance fields could be two large-scale numerical model forecasts, one valid at the current time and the other valid for the time of the detailed forecast. In the present application, we use forecasts provided by the National Meteorological Center's Limited-Area Fine-Mesh (LFM) model (Gerrity, 1977; Newell and Deaven, 1981) as our guidance fields. The high spatial resolution initial fields to which the model is applied are obtained from a Cressman (1959) objective analysis of hourly surface observations.

To date, most of the model applications have dealt with making 6-12 h forecasts of sea level pressure (SLP), although some work has been done for other variables such as surface wind, temperature, and moisture. The sample forecasts discussed in Section 3 are for SLP at the 6-12 h range.

2. FORECAST MODEL

If O_1 is the detailed initial field for, say, time one and F_1 and F_2 are the LFM forecasts valid at time one and time two, the Pattern Correlation Model (PCM) produces a detailed forecast for time two from the relation,

$$\tilde{O}_2 = \hat{O}_2 + (F_2 - \hat{F}_2). \qquad (1)$$

In Eq. (1), the detailed forecast is denoted $\tilde{O}_2$, $\hat{O}_2$ is the detailed initial field translated to time two using the field of translation vectors derived by the PCM from F_1 and F_2, and $\hat{F}_2$ is F_1 translated to time two using the same translation field. Note that the second term on the right side of Eq. (1) is the growth (along the flow) inherent in the LFM forecasts. Upon rearranging the right side of Eq. (1), we also see that,

$$\tilde{O}_2 = F_2 - (\hat{F}_2 - \hat{O}_2). \qquad (2)$$

From Eq. (2), we see that the detailed forecast at time two is the result of the large scale LFM forecast at time two minus the LFM error field at time one after translation to time two.

The essence of the PCM is the field of translation vectors derived from F_1 and F_2. Following the Clodman (1980) procedure, the translation vectors are derived by finding the best local pattern match between F_1 and F_2. The procedure involves making trial displacements of F_1 relative to F_2 over windows of the grid domain and testing each displacement for the best pattern match. The goodness of the match is expressed by the linear correlation coefficient. The displacement that yields the highest correlation defines the pattern translation over the time span separating F_1 and F_2.

The ultimate determination of the pattern translation embodied in the F fields is actually obtained after several iterations of the above procedure. The current estimate of the translation field obtained on a given iteration, ν, is applied to $\hat{F}_2^{(\nu-1)}$ (the translated F_1 field obtained with vectors from iteration $(\nu-1)$) to yield $F_2^{(\nu)}$. This translation field is improved on the next iteration $(\nu+1)$ as the local matching is repeated on the basis of $\hat{F}_2^{(\nu)}$ and F_2. On the first iteration $(\nu=1)$, the map patterns are matched within large windows to obtain an estimate of the large scale translation field. For our 44x58 grid, which has a mesh of 40-45 n mi, six large square overlapping windows (23x23 gridpoints) are used (Fig. 1). On the second and subsequent iterations, the patterns are matched within small circular windows (of radius four gridlengths) centered inside large square windows the same size as used in the first iteration (Fig. 2). In this dual window configuration, the $\hat{F}_2^{(\nu)}$ field is displaced only within the small circles, not over tha area between the circles and the borders of the large squares. As before, the correlation coefficients are computed from all points within the squares. This dual window configuration promotes both smooth convergence toward the final pattern match and spatial continuity in the translation vectors.

On our 44x58 grid, the network of small circular windows forms a 7x10 array (Fig. 2). We note that these circular windows are centered inside the large square windows everywhere except near the grid boundaries. This window configuration is essentially the same as the one used by Clodman, with the differences stemming from our larger grid domain and smaller grid mesh.

Within each window, F_1 is displaced 121 ways relative to F_2, $\pm$ 5 displacement increments in each grid direction. The displacement increment is one gridlength for all pattern matching iterations preceding the last, and one-half gridlength on the last. The smaller increment on the final iteration allows for a finer matching. Thus, the complete set of trial displacements results in an 11x11 matrix of correlation coefficients for each window. Note that the maximum possible pattern displacement within a window on any iteration is $\pm$ 5 gridlengths ($\pm$ 2 1/2 on the last iteration), which is provided for by the border space shown in Fig. 2. When the total displacement from two or more iterations exceeds this border space, points which fall outside the grid boundary are not used in the computation of the correlation coefficients for the windows involved.

On each iteration, the 7x10 array (2x3 array on the first iteration) of translation vectors must be interpolated and extrapolated to all points of the 44x58 grid. Although simple interpolation/extrapolation methods could be used, we applied the Cressman (1959) analysis method after it was modified to improve its performance in extrapolating data beyond the borders of the 2x3 and 7x10 array areas (see Appendix A). In the analysis procedure, only one pass with a scan radius of 32.0 gridlengths was used for interpolating the 44x58 grid from the 2x3 array of vectors, whereas 3 passes with scan radii of 20.0, 13.5, and 8.0 were used for the 7x10 arrays.

In our experiments with the 6- and 9-h translation fields, i.e., F_1 and F_2 separated by 6 and 9 hours, the matching procedure in almost all cases converged smoothly to a solution after three iterations. (The criterion for convergence is that the change in the current estimate of the translation vector with further iterations for any window is $\leq$ 2 grid lengths.) At 12 hours, the model occasionally had difficulty in meeting this criterion at a few windows with just three iterations, but the problem was not considered serious enough to warrent additional iterations.

The smooth and rapid convergence achieved by the model is aided by several built-in devices. One of these is conventional spatial smoothing using a nine-point Shuman (1957) filter. The smoother in two dimensions is given by,

$$Z_{I,J} = Z_{I,J} + [1/2\alpha(1-\alpha)](Z_{I+1,J} + Z_{I,J+1} + Z_{I-1,J} + Z_{I,J-1} - 4Z_{I,J}) + [1/4\alpha^2] (Z_{I+1,J-1} + Z_{I+1,J+1} + Z_{I-1,J+1} + Z_{I-1,J-1} - 4Z_{I,J}), \quad (3)$$

where $Z_{I,J}$ is the smoothed value of the scalar variable Z at gridpoint I,J (I and J increase toward right and top of grid) and α is a smoothing parameter. This smoother was applied (a) to the F_1 and F_2 fields prior to the pattern matching analysis, (b) to the 11x11 matrices of correlation coefficients, and (c) to the 7x10 arrays of translation vector corrections obtained on the second and third iterations and to the final vectors obtained with the third iteration. The parameter, α, for these smoothing applications had values of 1.0 for the F_1 and F_2 fields, $\geq$ 0.9 for the correlation matrices, and $\geq$ 0.4 and $\geq$ 0.3 for the vector corrections and final vectors, respectively. The reason for the inequality preceding the last three values is that α actually varies over the array being smoothed according to b/r, where b is equal to the values given (0.9, 0.4, and 0.3) and r is the correlation coefficient corresponding to the pattern match between F_1 and F_2. (Since most correlation coefficients are above 0.9, the values of α are usually not much larger than b.) The idea is to smooth the correlation coefficients and translation vectors more where the pattern match is poor and less where it's good. We note that the spatial smoothing of the 11x11 correlation matrices is not as simple as the other smoothing application. For instance, the nine correlation values involved in a smoothing computation are taken from nine correlation matrices corresponding to a 3x3 set of neighboring windows. The central point is, of course, an element of the matrix being smoothed, while the remaining eight points come from corresponding elements of the eight surrounding matrices. Thus, the smoothing is performed over correlation coefficients from neighboring windows with the same trial displacement.

Another device that assists in the smooth, rapid convergence to a solution is an empirical modification of the smoothed correlation matrix. For iterations two and three, as corrections (or adjustments) to existing translation vectors are being made, two modifications are made to the matrix. First, the quantity 0.00003 is added to the coefficient corresponding to zero vector adjustment (i.e., no displacement of $\hat{F}_2^{(\nu)}$ relative to F_2). Then the quantity $0.00025d^2$ is subtracted from each element of the matrix, where d is the displacement distance in gridlengths between $\hat{F}_2^{(\nu)}$ and F_2. These modifications act to discourage large vector corrections for windows with weak gradients in the correlation matrix.

Finally, smoothing or constraining devices are applied to suspect translation vector estimates after iterations two and three. The selective smoothing procedure replaces a vector correction on the third iteration with a weighted average of the corrections from the second and third iterations when the change

in these corrections exceeds five gridlengths. The weights are 60/40 in favor of the correction on the third iteration. This smoothing procedure was designed to suppress excessive forward-backward oscillations in the vector corrections between the iterations. We have found, however, that this inter-iteration smoother is very rarely used with F_1 and F_2 separated by 6 or 9 hours. It's used less rarely at 12 hours. When this smoother is invoked, it assists in the convergence toward a solution. The situation in which it may be called upon is usually one in which the F_1 and F_2 fields exhibit weak gradients, are poorly organized, and are simultaneously undergoing great changes.

The selective vector constraining device consists of a downward adjustment to the magnitude of a translation vector on iterations two and three when it exceeds a certain threshold. This threshold is 3.5 gridlengths for 6-h vectors, 4.3 gridlengths for 9-h vectors, and 7.0 gridlengths for 12-h vectors. Plots of the modified and unmodified vector magnitudes for 6, 9, and 12 hours are shown in Fig. 3. The 12-h curve, for example, is defined as,

$$y = x \quad , \; x \leq 7$$
$$y = 2.5 \, \mathrm{Tan}^{-1} \, 2/5x \; , \; 7 < x \leq 13.4$$
$$y = 10 \quad , \; x > 13.4 \; ,$$

where y and x are the modified and unmodified vector magnitudes in gridlengths. The 6- and 9-h curves are similarly defined. Note from Fig. 3 that this adjustment truncates 6-h unmodified vectors $\geq$ 6.8 gridlengths to 5.0 gridlengths, 9-h vectors $\geq$ 9.6 gridlengths to 7.5 gridlengths, and 12-h vectors $\geq$ 13.4 gridlengths to 10.0 gridlengths. These upper vector bounds equate to a maximum allowable speed of about 38 kt. While this speed limit may seem somewhat low, two factors should be considered. One is that the features forecast by the LFM are of the synoptic scale whose phase speeds may not be as large as those occasionally exhibited by smaller scale features such as cold fronts or squall lines. Also, one must weigh the drawback of introducing slight error in some correct vectors against the greater benefit of removing large error in some incorrect vectors.

We note that the smoothing and vector constraining procedures employed here represent significant departures from and extensions to Clodman's model. They were introduced primarily to speed up convergence to a satisfactory solution, which they did. Clodman used eight iterations to achieve the solution, which becomes too computationally expensive for the grid we used.

3. FORECAST PERFORMANCE

In this section, we examine the PCM's performance in producing 6-, 9-, 12-h forecasts of sea level pressure (SLP). First, the workings of the model are illustrated by examining one case in detail. We then summarize the forecast performance for 22 selected cases. Almost all of the cases featured a major developing cyclonic system within the grid area.

The initial time of the PCM forecasts in all cases was 2100 GMT. The driving forecasts from the LFM were initialized at 1200 GMT of the same day. Thus, for the 6-h PCM forecast valid at 0300 GMT of the next day, the LFM guidance forecasts are valid at 2100 and 0300 GMT. For the 9-h forecast valid at 0600 GMT, the LFM forecasts are valid at 2100 and 0600 GMT. Finally, for the 12-h forecast valid at 0900 GMT, the LFM forecasts are valid at 2100 and 0900 GMT. The LFM SLP forecasts at these projections were obtained by first fitting a quadratic function to 12-hourly forecasts for projections of 0, 12, 24, and 36

hours at each gridpoint[1]. The forecast values at the required projections were then interpolated from the quadratic functions. This procedure serves not only in providing forecasts at the projections needed, but it performs temporal smoothing. The smoothing feature is quite desirable since it would reduce temporal oscillations possibly present in the forecasts at the shortest projections as a result of LFM model imbalances with the initial states.

The case selected for detailed examination is for 8-9 April 1979. The weather for this case featured numerous tornadoes and severe thunderstorms in the Mississippi Valley. The interpolated 9-, 15-, 18-, and 21-h LFM forecasts from 1200 GMT 8 April are shown in Figs. 4a-4d. Note that the cyclonic system centered in Indiana and Ohio deepened as it moved eastward. The pattern translation and growth fields derived by the PCM from the 9-15, 9-18, and 9-21 h LFM forecasts are shown in Figs. 5a-5c and Figs. 6a-6c, respectively. It is encouraging that the translation and growth patterns for these 6-, 9-, and 12-h periods are similar since the PCM solutions for these periods are independent of each other. The slight reduction in translation speed from the 6- to the 12-h period over the eastern United States reflects an apparent slowing with time in the eastward movement of the system. The 6-, 9-, and 12-h forecasts obtained by applying the translation and growth patterns to the detailed initial field (Fig. 7) are shown in Figs. 8a-8c. Comparison of these forecasts with the verifying analyses (Figs. 9a-9c) reveals good correspondence in the major features.[2]

Inspection of the forecast error maps shown in Figs. 10a-10c reveals three major error centers. One is over the Applachian Mountains, another over Arkansas, and a third over Utah. These errors basically reflect errors in the LFM forecasts. For instance, a comparison of Figs. 4 and 9 shows that the LFM was too slow in the movement of the trough that extended from Indiana to northeast Texas at 2100 GMT 8 April. Fig. 9 shows that this trough moved rapidly eastward with strong ridging to the west, resulting in the positive and negative error centers in the southeastern states. The large positive error over Utah resulted from the LFM not correctly forecasting the strong observed pressure falls in this area, especially evident from 2100 GMT 8 April to 0300 GMT 9 April in Figs. 8a-8b. Note from Fig. 10 that the PCM forecast errors grew smoothly from the 6- to the 12-h period.

Table 1 gives the mean absolute error, rms error, and S1 score for the PCM and LFM guidance forecasts for the 8-9 April 1979 case as computed over the area shown in Fig. 2. For comparison, Table 1 also gives average scores from the 22 cases which were selected primarily from the winter and spring seasons of 1977-81.

---

1 We also tried using 6-hourly SLP guidance fields obtained from available 6-hourly 1000-mb height forecasts after an appropriate conversion was applied. (SLP forecasts directly output from the LFM were availabe only at 12-h intervals.) Verification statistics based on 17 cases showed that the derived 6-hourly SLP fields resulted in very slightly poorer PCM forecasts than those based on the 12-hourly SLP forecasts directly output by the LFM.

2 The PCM forecasts are slightly smoother than the initial and verifying fields since light smoothing was applied. The smoothing consisted of two passes of the nine-point filter with smoothing parameter values of 0.4, 0.7, and 1.0 for the 6-, 9-, and 12-h forecast fields, respectively.

We see that the scores of the PCM and LFM on 8-9 April were not greatly different from the 22-case average. In the average scores, the large PCM improvement over the LFM seen at 6 hours has largely disappeared by 9 hours, especially in the S1 score. By 12 hours, the LFM is slightly ahead of the PCM in the S1 score but not in the mean absolute and rms errors. The reason the LFM fared better in the S1 score lies in the relative smoothness of the PCM and LFM forecast patterns. The smoother LFM forecasts tend to produce better S1 scores when verified against a detailed analysis.

Subjective evaluation of the PCM forecasts over the 22 cases produced some interesting findings. In general, we found that the forecasts were quite accurate in those cases that did not exhibit large changes in the shape of the SLP pattern. This was true even when the major cyclone underwent strong deepening. However, in many of these synoptically-active cases, the observed strong amplification of the trough-ridge pattern was accompanied by significant changes in the pattern shape. For instance, a developing cyclone often exhibited strong troughing to the east of the low center in conjunction with a warm front and strong ridging to the southwest behind a sharp cold front. The PCM forecast characteristically failed to capture the full extent of the troughing and ridging. The forecast error pattern in such instances gave the impression of erroneously slow movement of the system.

The forecast error in such cases was determined to result from two problems. One is that much of the cyclonic/anticyclonic development in the initial and verifying SLP fields is of a small scale and, therefore, not well resolved in the LFM forecasts. Since the PCM extracts the pattern translation and development from the LFM forecasts, scales not resolved by the LFM are not properly handled. The other problem is that even when the LFM does a good job of forecasting strong pattern changes the PCM generally does not fully reflect the deformation in derived translation vector field. That is, in those cases for which the LFM forecast significant pattern change during cyclonic development, the PCM translation field usually did not fully reflect the changes. This is in spite of the fact that the translation vectors exhibited less than a 5% overall slow bias, as revealed by a comparison of 77 hand-calculated vectors against the model vectors over the 22 cases. Experiments have shown that just one additional iteration removes some of the error. Still better account of strong pattern changes would require more iterations using windows of decreasing size, but the amount of additional computation would be quite substantial.

The PCM forecasts also revealed a systematic "error" over the western United States resulting from the arbitrary pressure reduction to sea level. Pressure reduction techniques over mountainous terrain often result in fictitious stationary SLP features. The PCM tended to displace such features in accordance with the LFM guidance forecasts resulting in "error" when the forecasts were compared with the verifying analysis. No attempt was made to deal with the pressure reduction problem.

4. CONCLUSIONS AND REMARKS

The PCM model, described in detail in this note, appears to be useful for updating LFM sea level pressure forecasts for projections to at least 9 hours after data time. By 12 hours, the PCM forecasts appear to add nothing to the accuracy of the LFM forecasts which were used to drive the PCM.

An attractive feature of the PCM model is its potential versatility. For instance, the model can produce a detailed forecast of any variable for which appropriate initial fields and LFM forecasts are available. Also, the translation field alone, as based on some LFM forecast variable or product could be used to project a variety of meteorological fields 6-12 hours into the future, perhaps even those based on radar or satellite data. A significant limitation of the model is that it does not perform well when large pattern changes occur. Still, the accuracy of the forecasts are at least competitive with other simple models (see Charba and Jendrowski, 1981).

Another significant aspect of the model is its computational efficiency. A forecast covering the area shown in Fig. 2 requires about 1.5 minutes central processor time on the National Oceanic and Atmospheric Administration's IBM 360/195 computer. While this computing requirement rules out large-area applications of the model on local minicomputers, applications for regional areas may be quite feasible.

5. ACKNOWLEDGEMENTS

We wish to acknowledge helpful conversations with David A. Unger, Wilson A. Shaffer, and Paul E. Long, Jr.

6. REFERENCES

Charba, J. P., and P. A. Jendrowski, 1981: A comparison of 6-12 h forecasts of atmospheric surface variables using pattern correlation and other simple models. To appear in Preprints of the Twelfth Conference on Severe Local Storms, San Antonio, Amer. Meteor. Soc.

Clodman, S., 1980: Short-range forecasting using pattern correlation. Preprints Eighth Conference on Weather Forecasting and Analysis, Denver, Amer. Meteor. Soc., 474-477.

Cressman, G. P., 1959: An operational objective analysis system. Mon. Wea. Rev., 87, 367-374.

Gerrity, J. F., 1977: The LFM model-1976: A documentation. NOAA Technical Memorandum NWS NMC-60, National Oceanic and Atmospheric Administration, U.S. Department of Commerce, 60 pp.

Newell, J. E., and D. G. Deaven, 1981: The LFM-II model--1980. NOAA Technical Memorandum NWS NMC-66, National Oceanic and Atmospheric Administration, U.S. Department of Commerce, 20 pp.

Shuman, F. G., 1957: Numerical methods in weather prediction. II. Smoothing and filtering. Mon. Wea. Rev., 85, 357-361.

Table 1. Verification scores for the PCM and LFM forecasts for (a) 8-9 April 1979 and (b) for 22 cases from the winter and spring seasons of 1977-81. The 6-, 9-, and 12-h PCM forecasts are valid at the same time as the 15-, 18-, and 21-h LFM forecasts, respectively.

Model	Forecast Projection (h)	Mean Absolute Error (mb)	RMS Error (mb)	S1 Score
		(a) 8-9 April 1979		
PCM (LFM)	6 (15)	1.16 (1.83)	1.44 (2.19)	45.3 (56.1)
PCM (LFM)	9 (18)	1.58 (1.96)	2.04 (2.35)	52.6 (54.7)
PCM (LFM)	12 (21)	2.31 (2.52)	2.98 (3.10)	58.0 (57.5)
		(b) 22 Cases		
PCM (LFM)	6 (15)	1.87 (2.72)	2.36 (3.26)	43.9 (53.7)
PCM (LFM)	9 (18)	2.39 (2.89)	3.09 (3.47)	51.5 (53.7)
PCM (LFM)	12 (21)	2.84 (3.07)	3.72 (3.76)	57.6 (54.7)

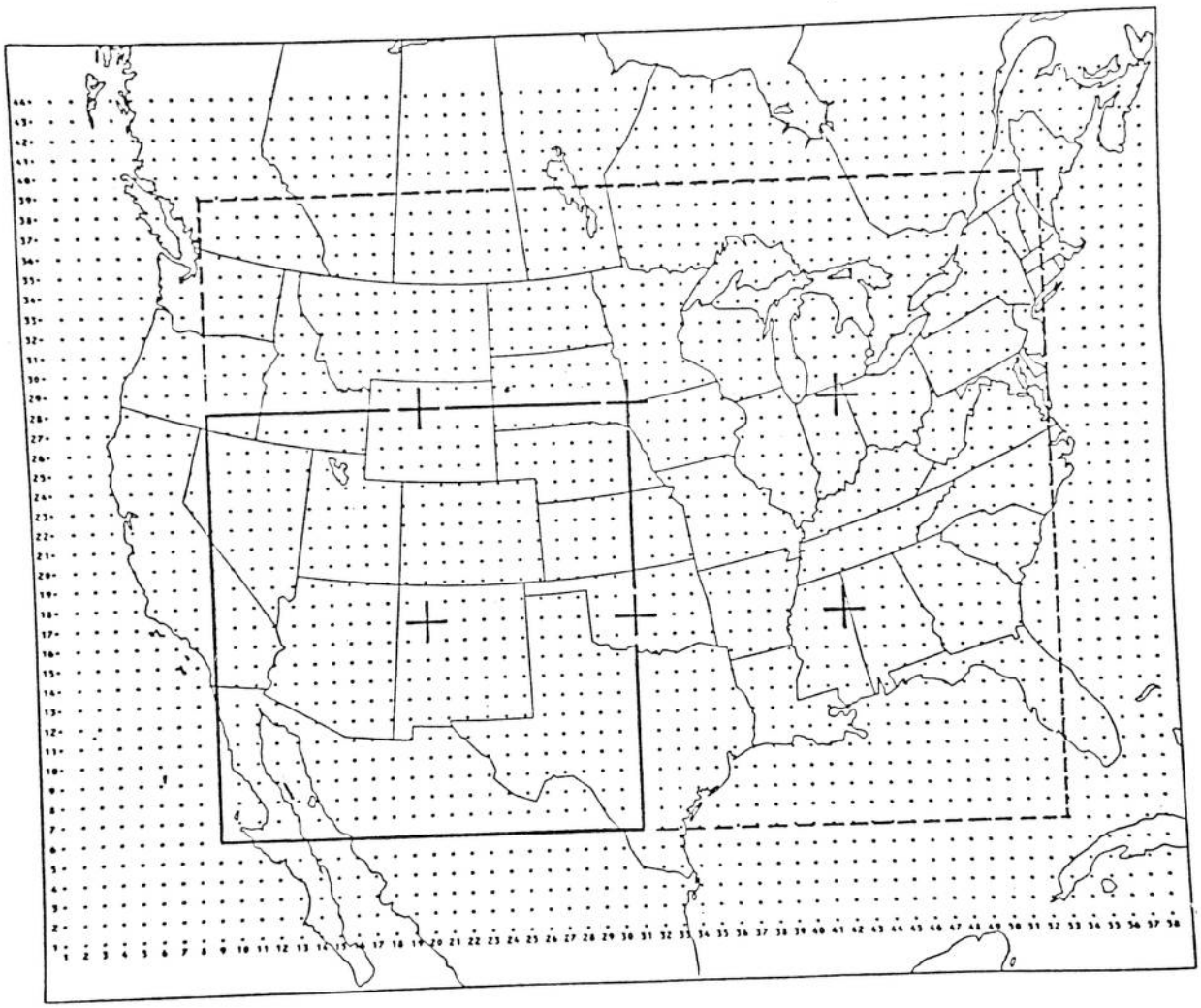

Figure 1. Computational grid with large square pattern-matching windows illustrated. The centers of the six large square windows used on the first iteration are indicated by the large crosses. The lower left square is shown with bold solid lines. The outer rectangle bounded by dashed lines is the area covered by these windows.

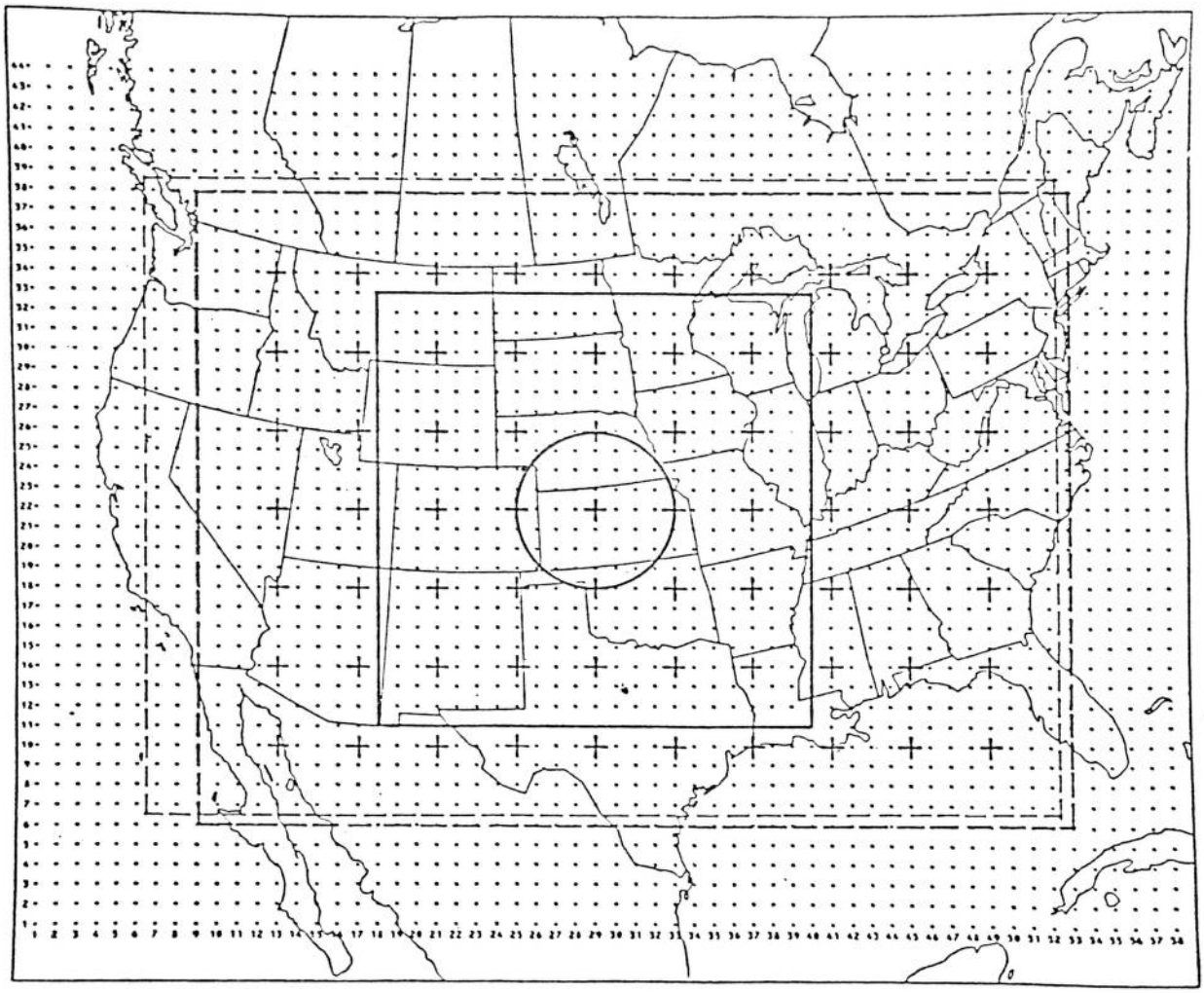

Figure 2. Computational grid with dual pattern-matching windows illustrated. The large square with the inscribed circle centered over Kansas depicts one of the dual windows that make up the 7x10 array. The centers of the small circles within the windows are depicted as the array of bold crosses. The area covered by the dual windows is denoted by bold dashed lines. The area bounded by the light dashed lines is the area over which the PCM and LFM forecasts are verified.

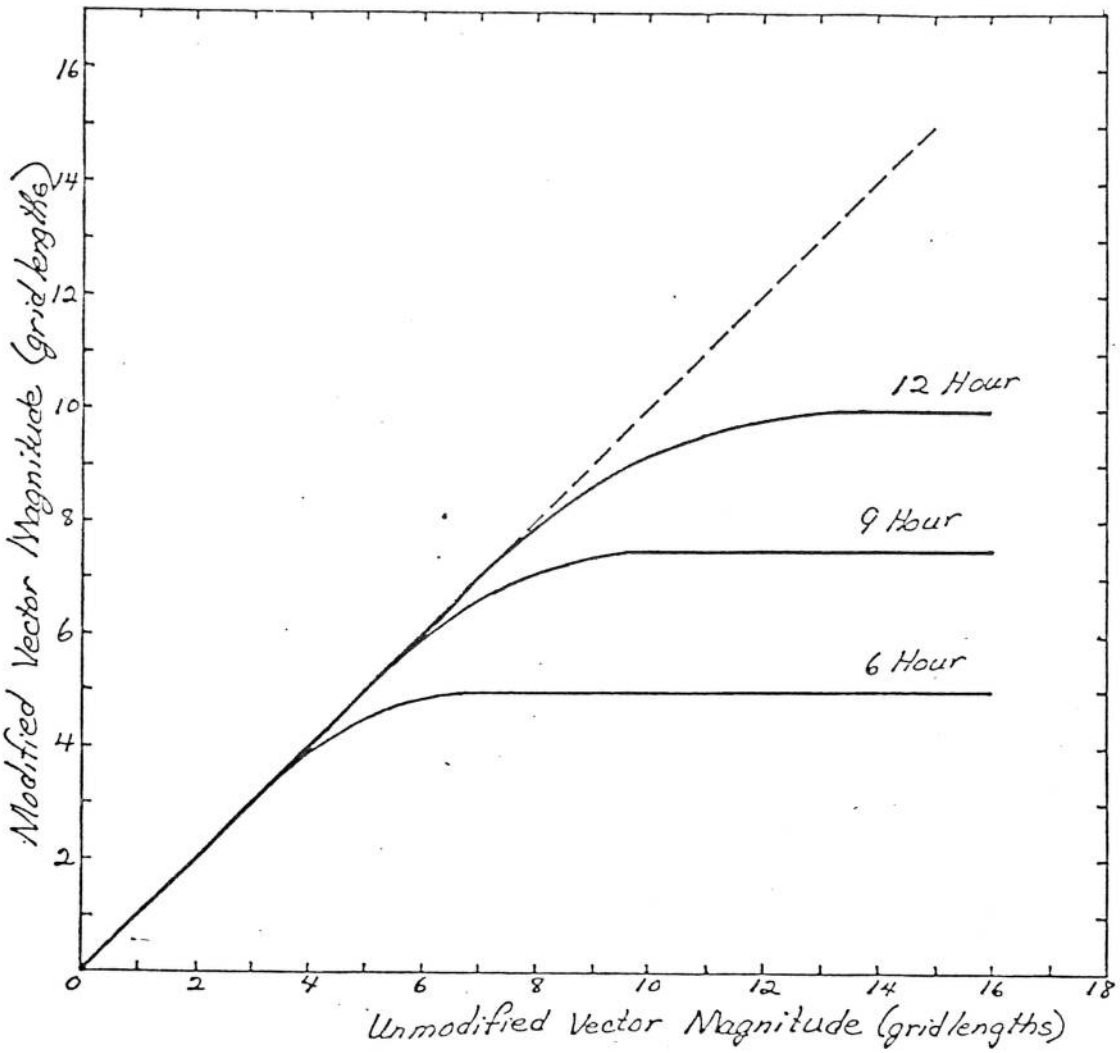

Figure 3. The relationship of the modified to the unmodified vector magnitudes for 6-, 9-, and 12-h vectors.

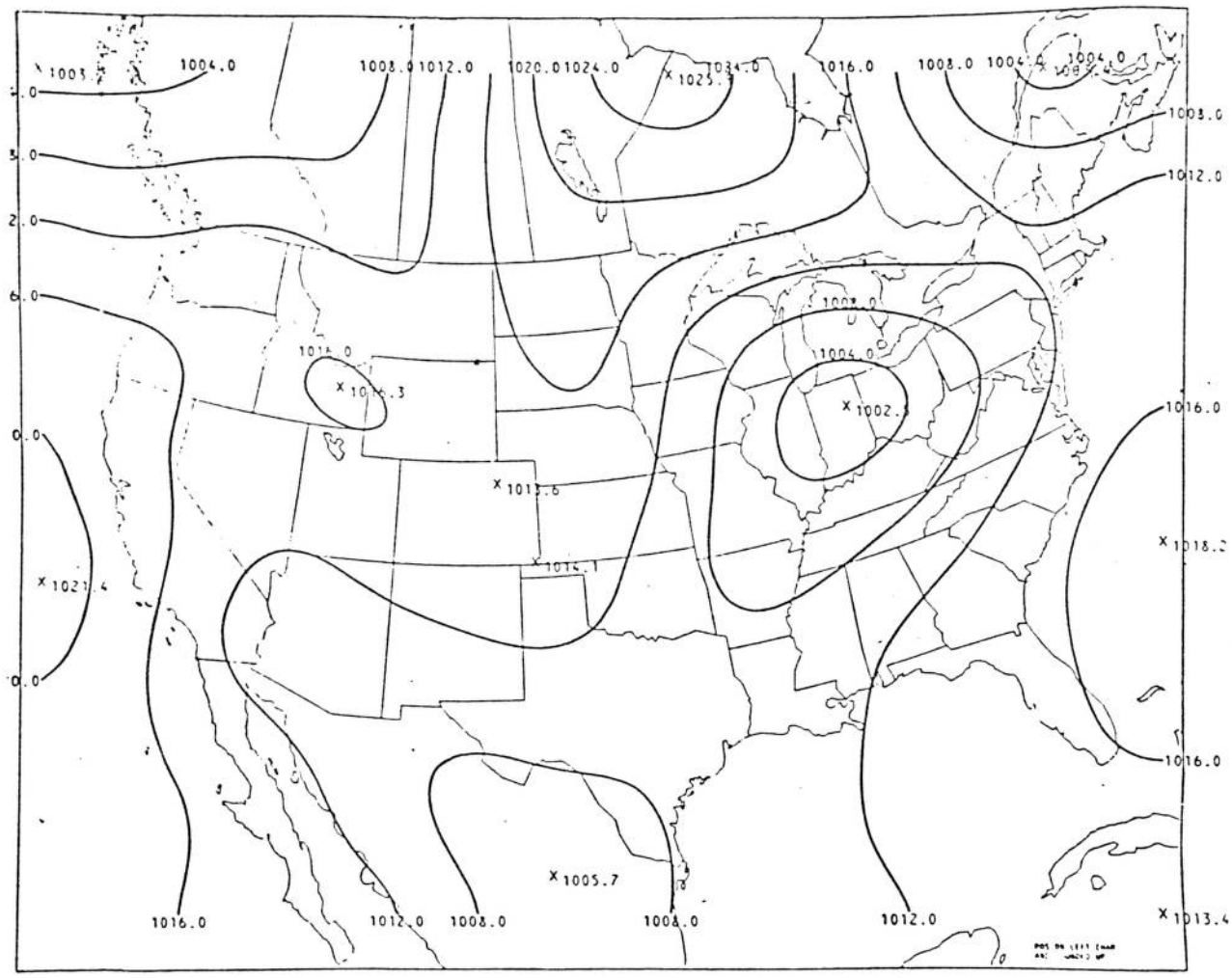

Figure 4a. Nine-hour LFM SLP forecast valid 2100 GMT 8 April 1979.

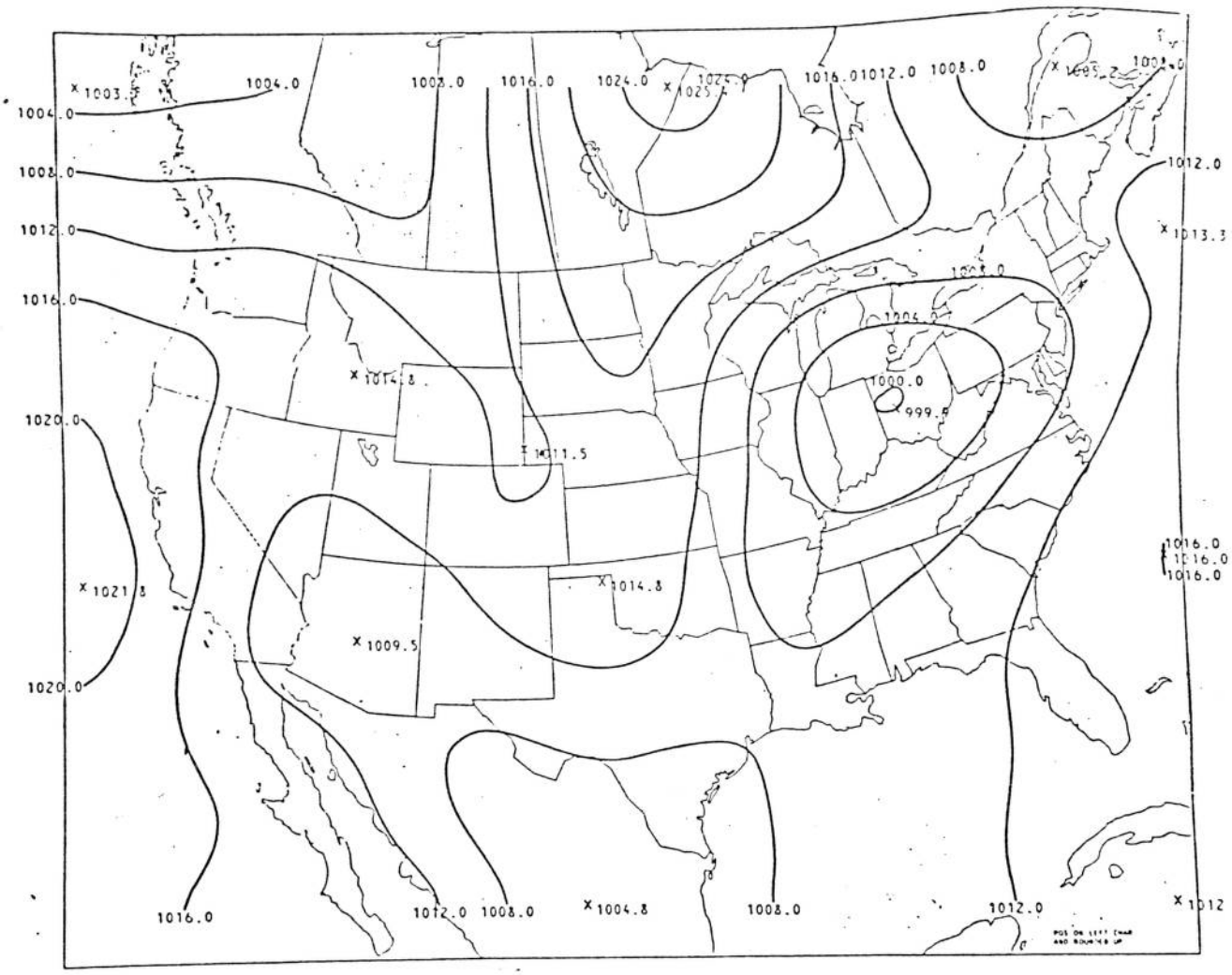

Figure 4b. Fifteen-hour LFM SLP forecast valid 0300 GMT 9 April 1979.

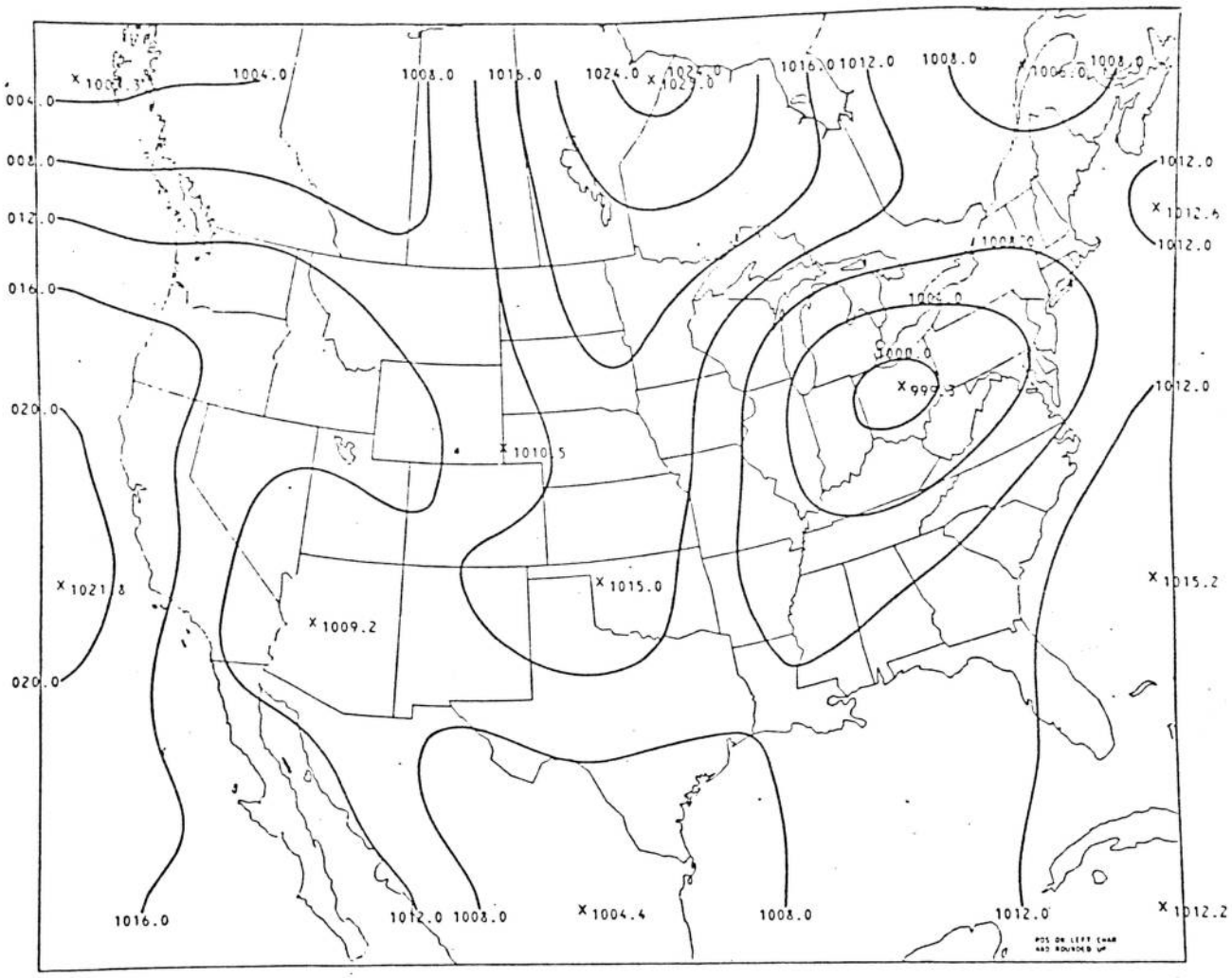

Figure 4c. Eighteen-hour LFM SLP forecast valid 0600 GMT 9 April 1979.

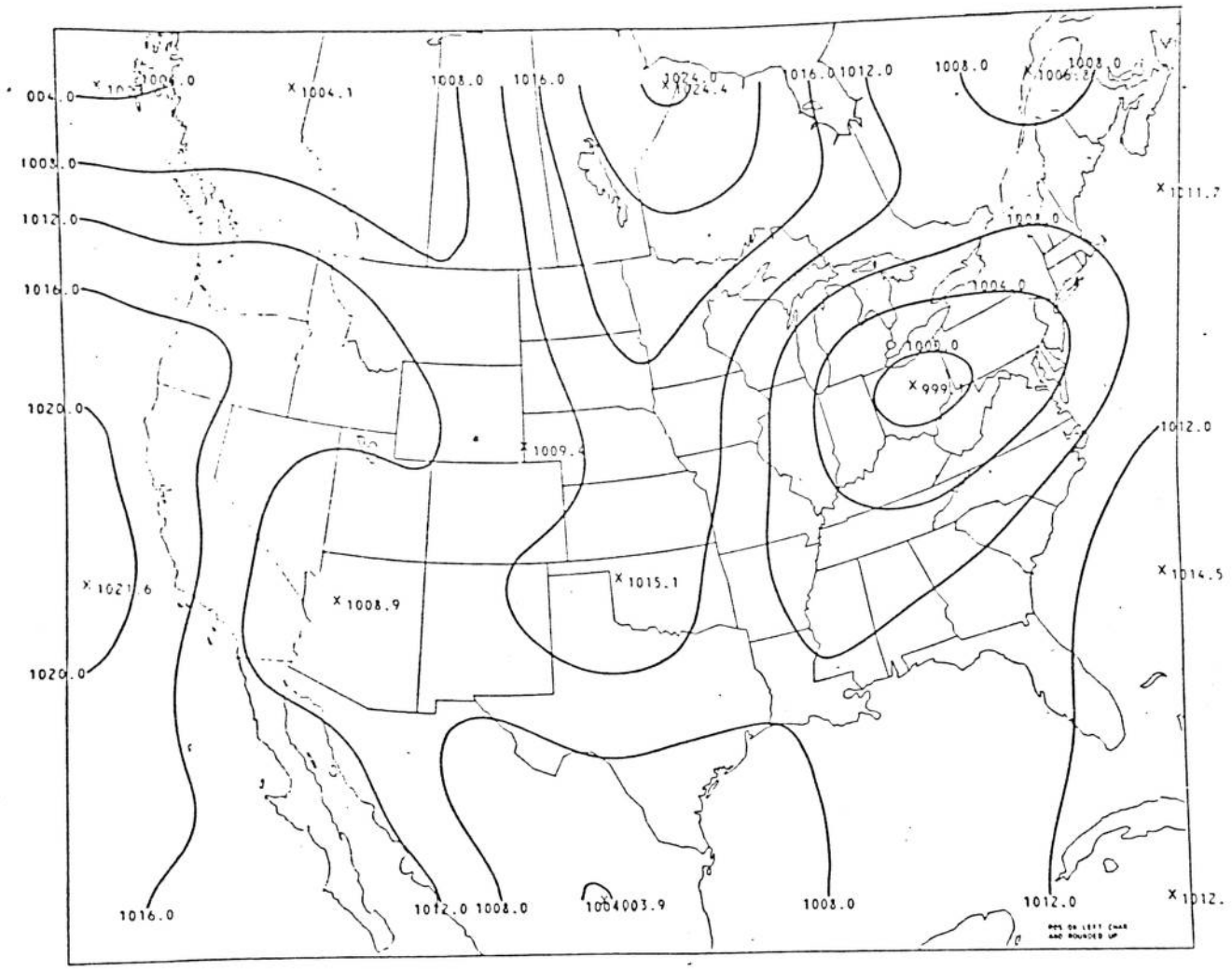

Figure 4d. Twenty-one hour LFM SLP forecast valid 0900 GMT 9 April 1979.

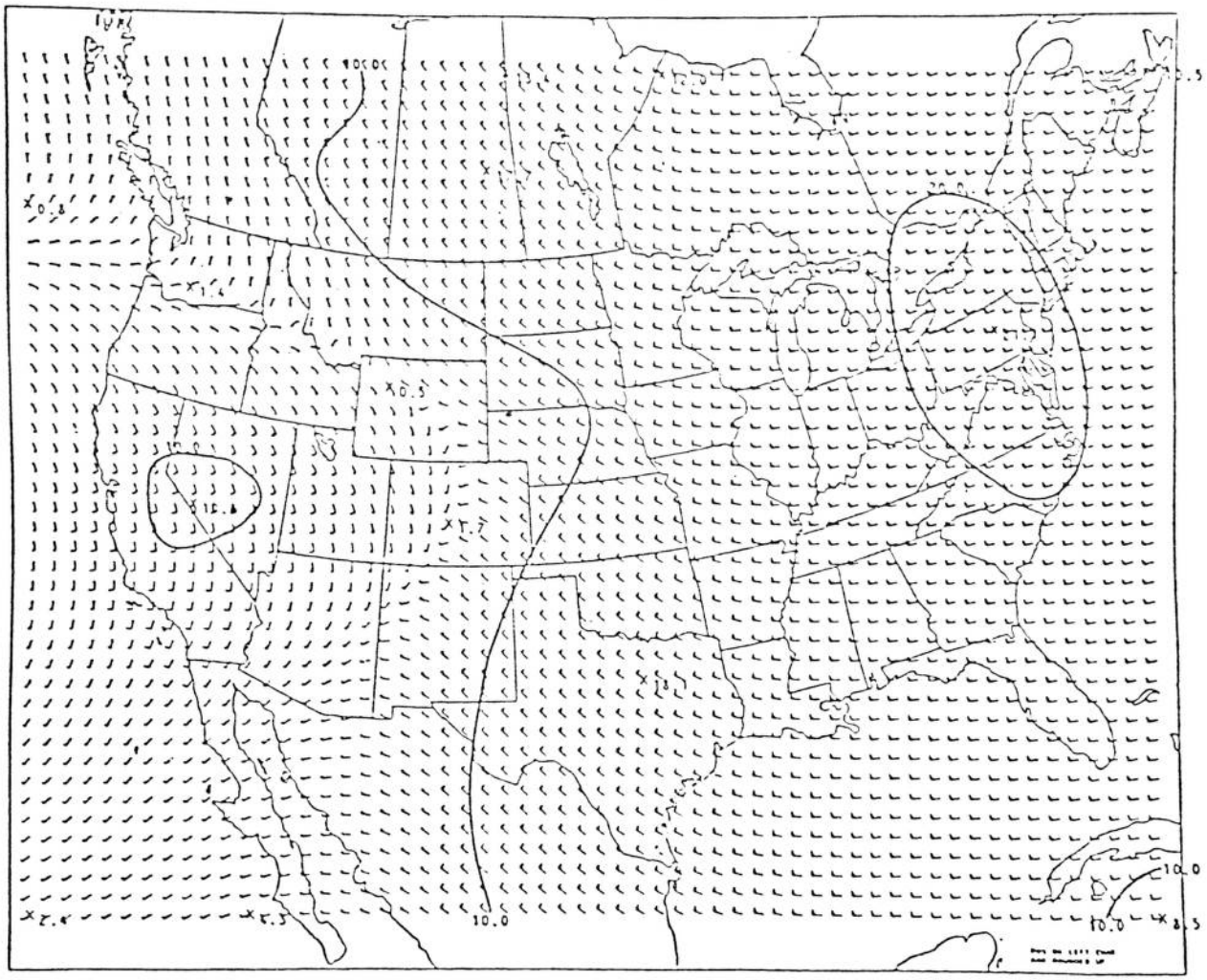

Figure 5a. Translation speed (one barb = 10 kt) and direction based on the 9-15 h LFM SLP forecasts.

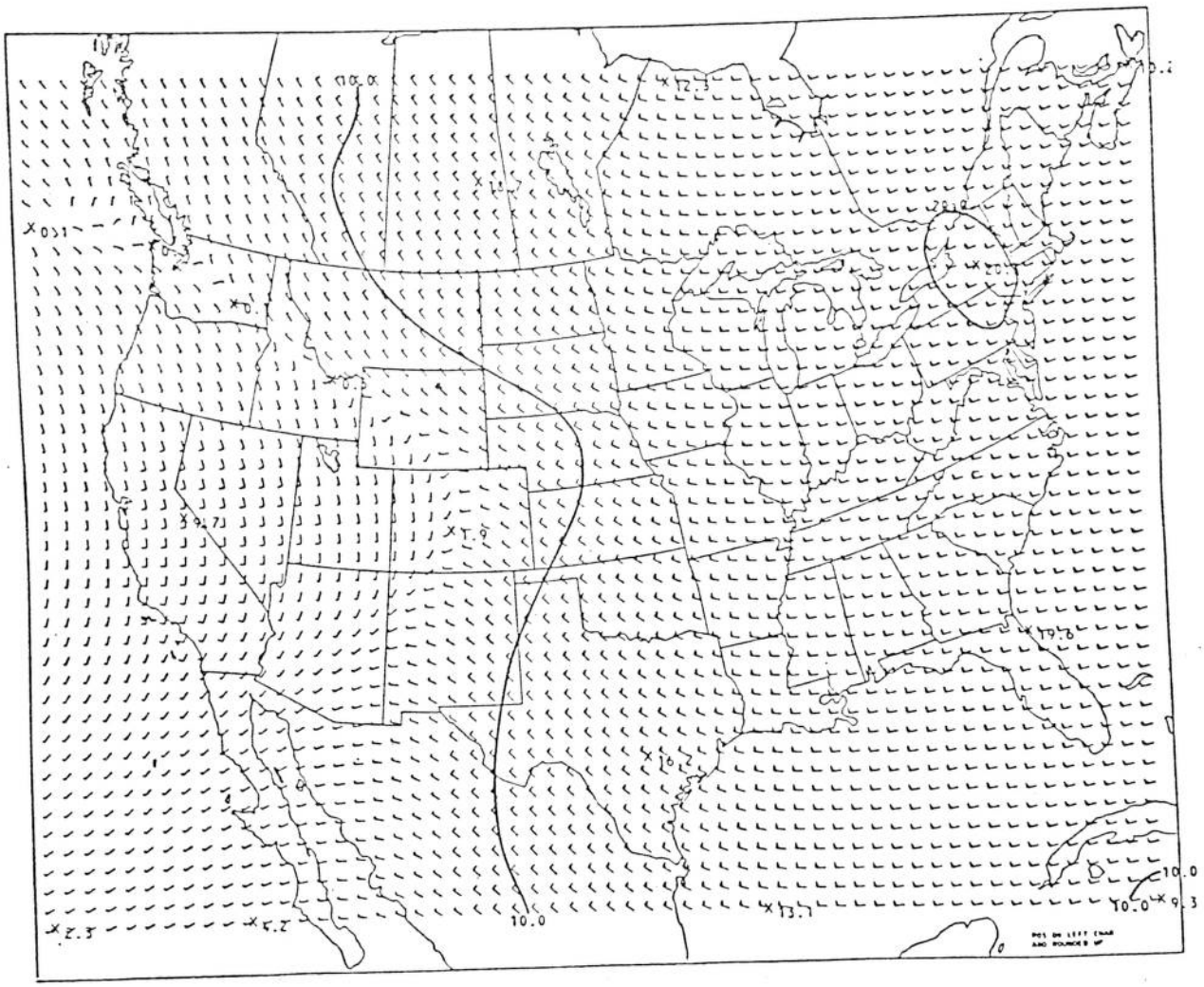

Figure 5b. Same as Fig. 5a for the 9-18 h LFM SLP forecasts.

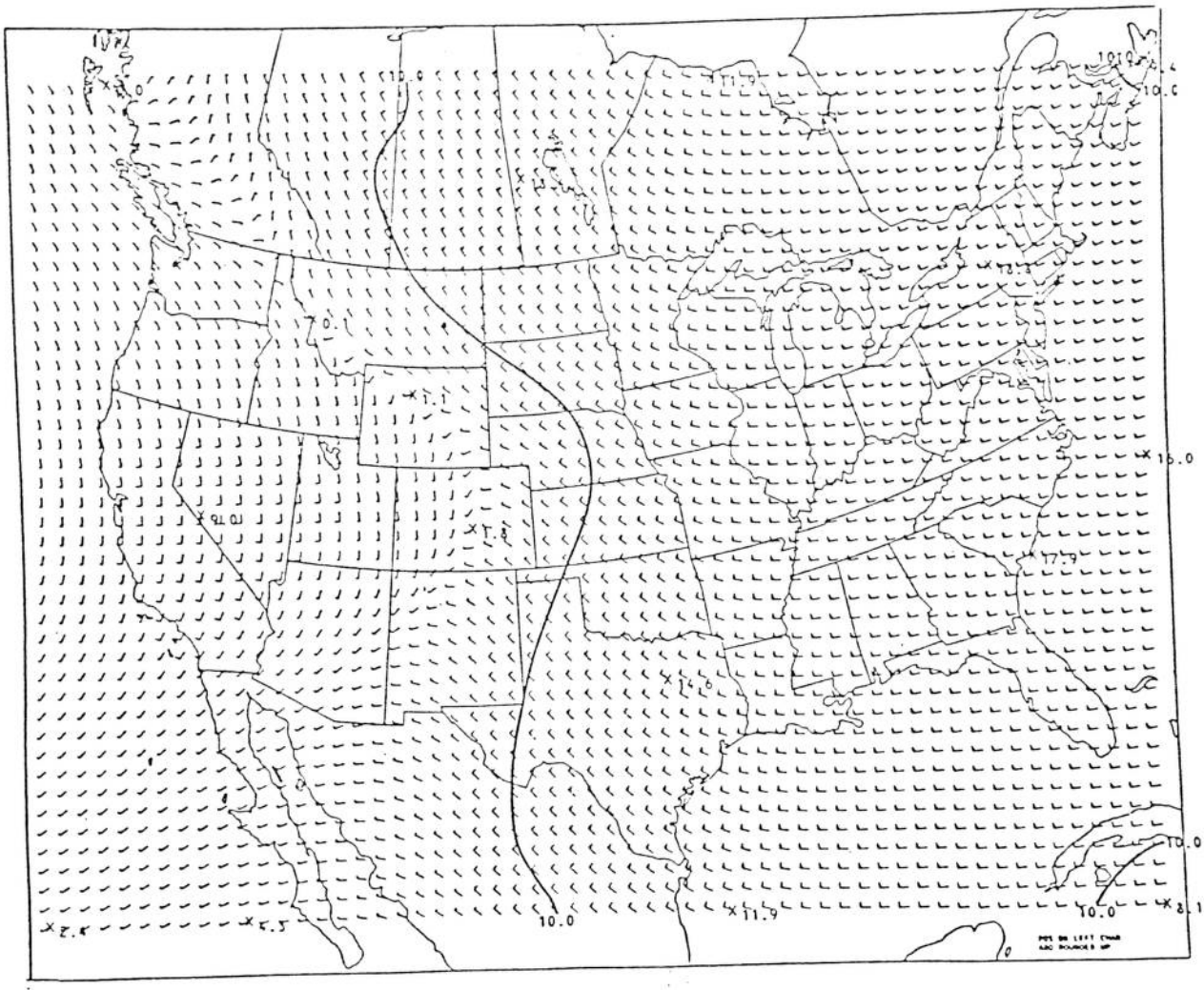

Figure 5c. Same as Fig. 5a for the 9-21 h LFM SLP forecasts.

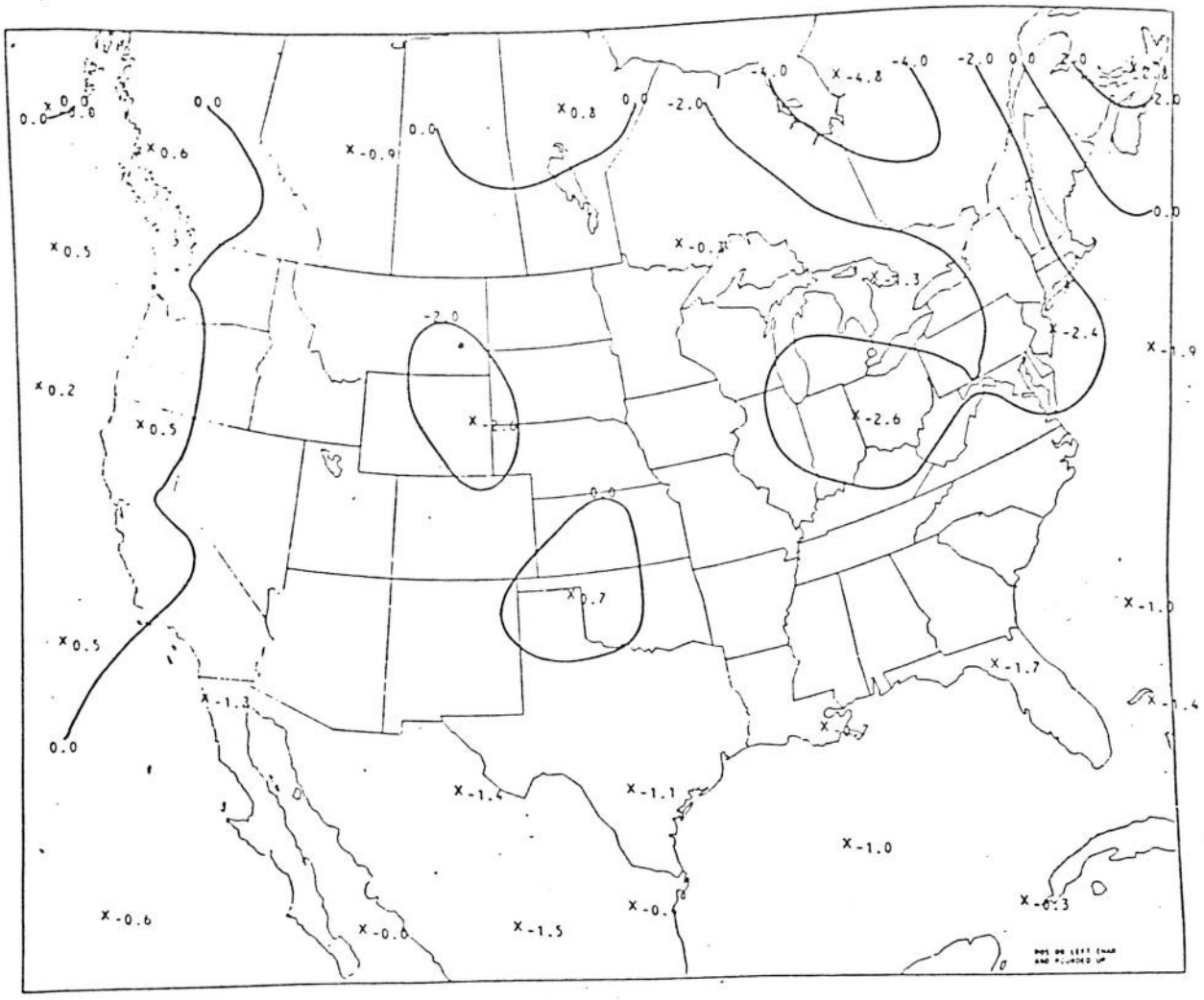

Figure 6a. Six-hour growth field (mb) corresponding to Fig. 5a.

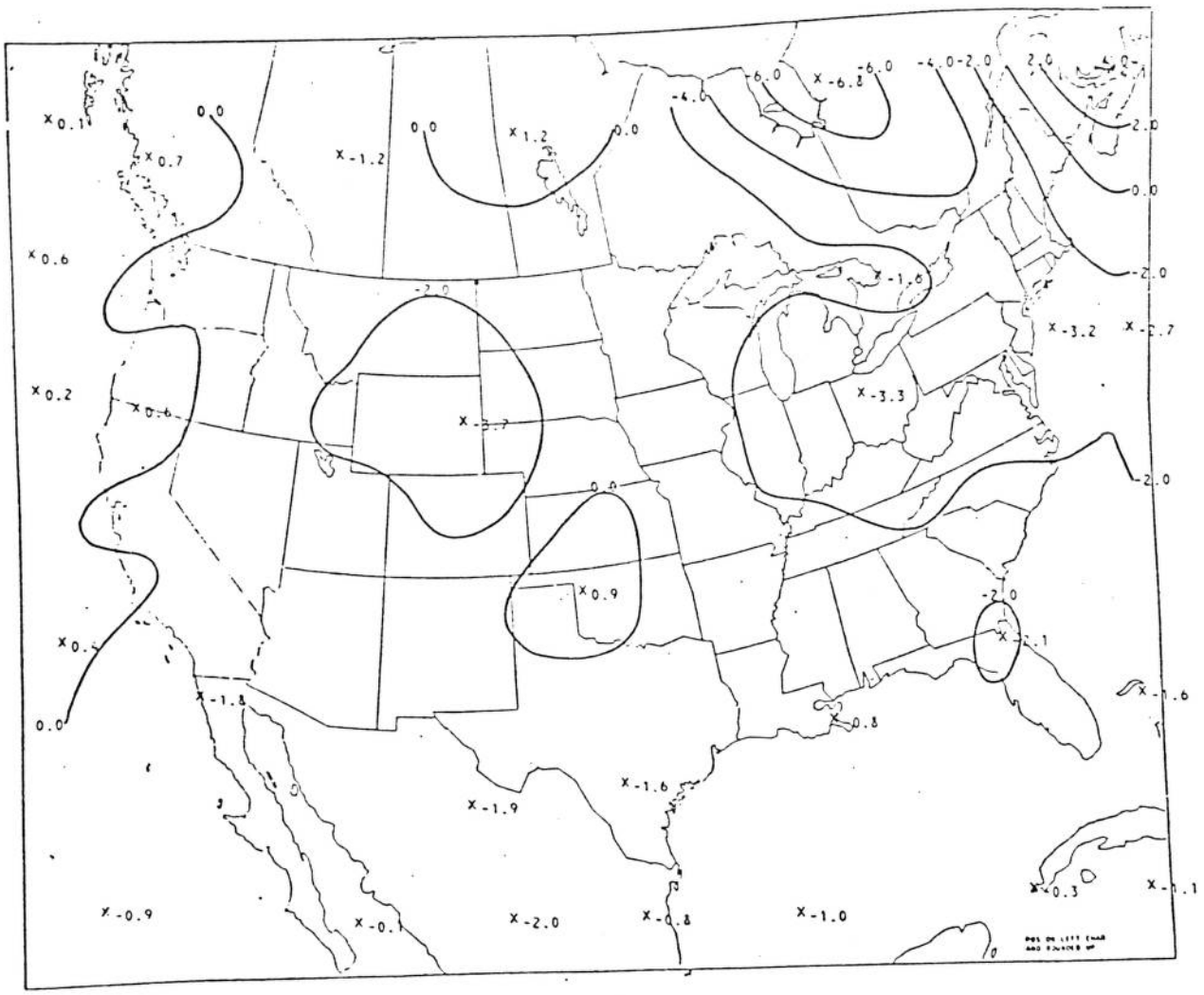

Figure 6b. Nine-hour growth field (mb) corresponding to Fig. 5b.

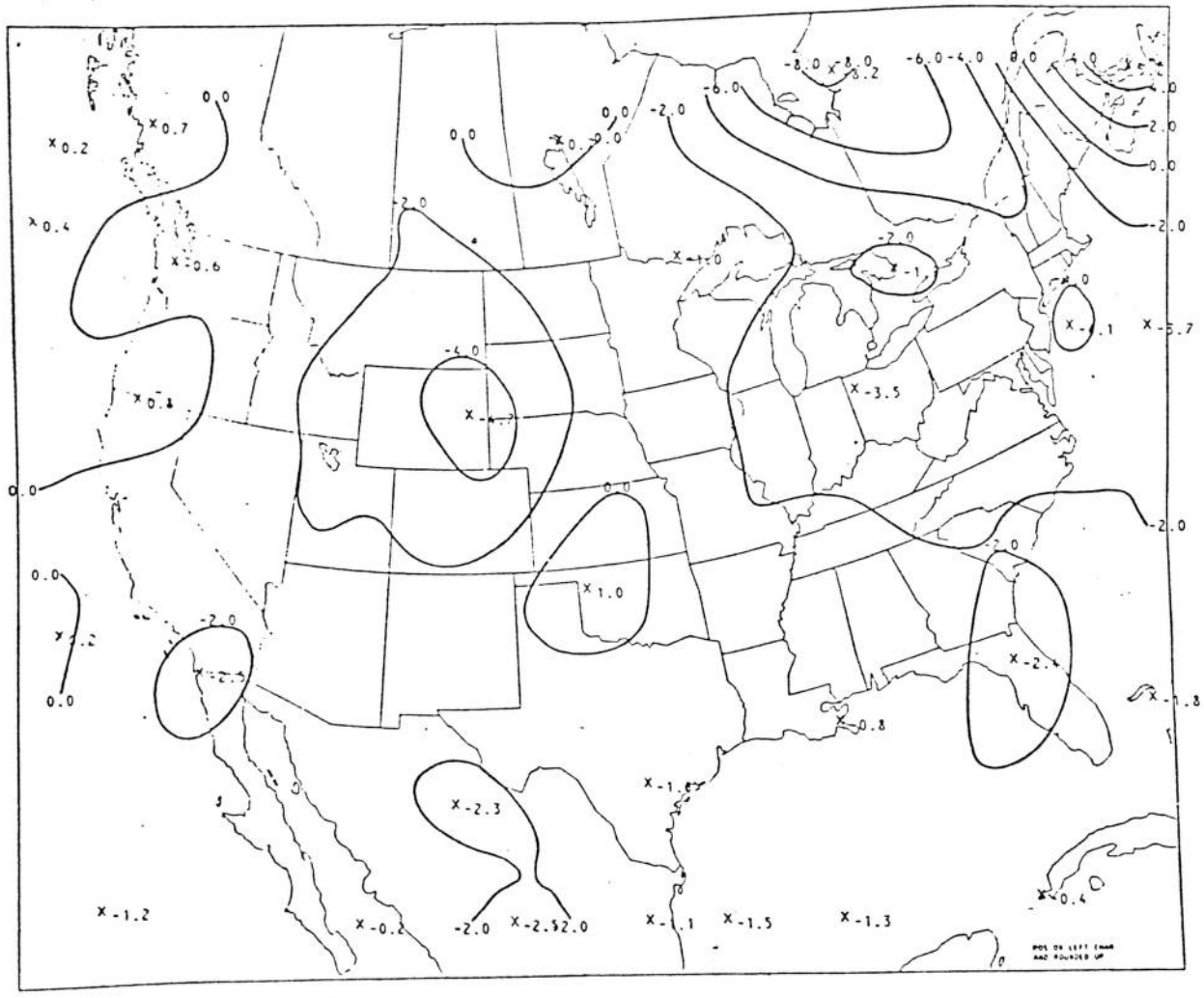

Figure 6c. Twelve-hour growth field (mb) corresponding to Fig. 5c.

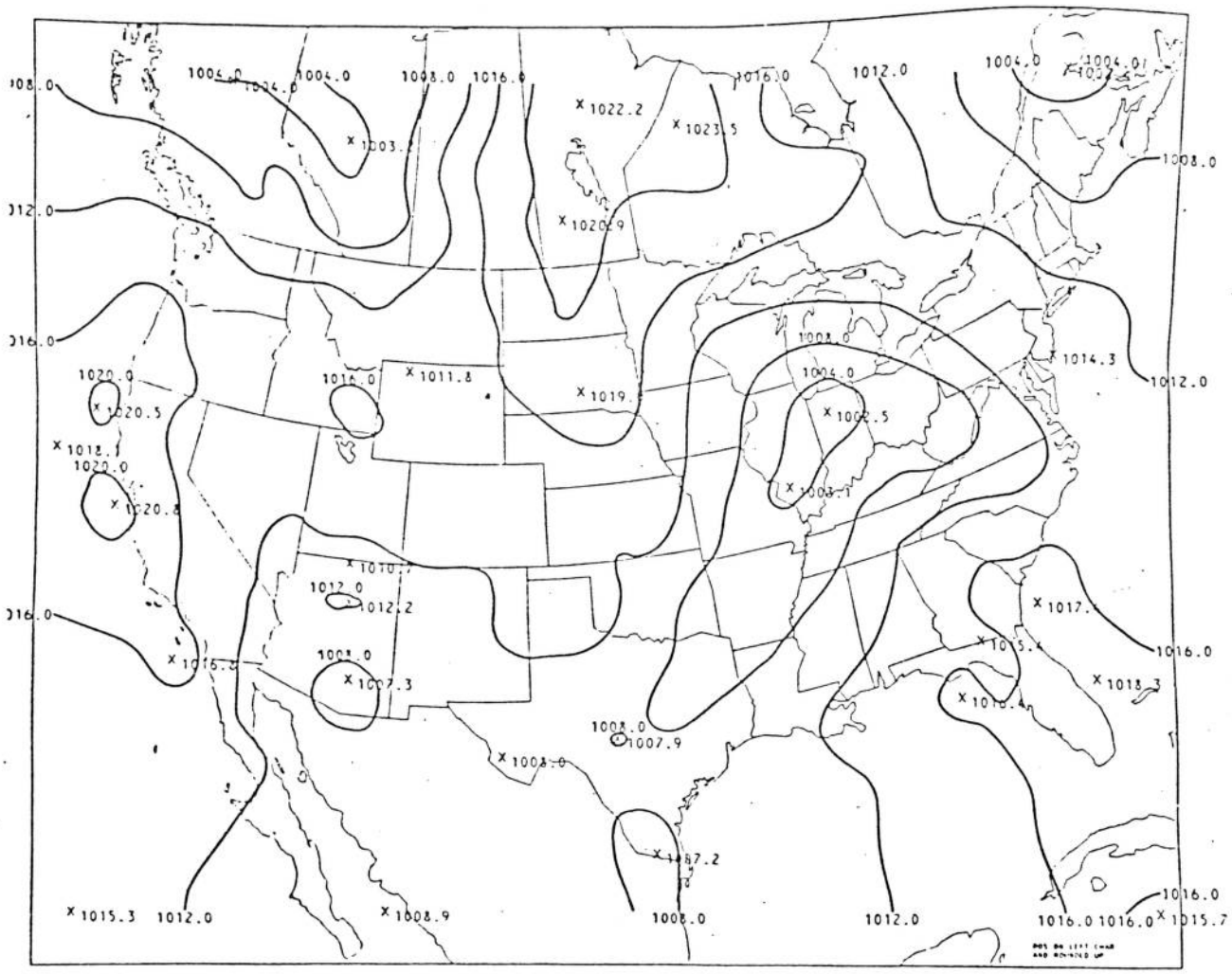

Figure 7. Initial SLP field valid 2100 GMT 8 April 1979.

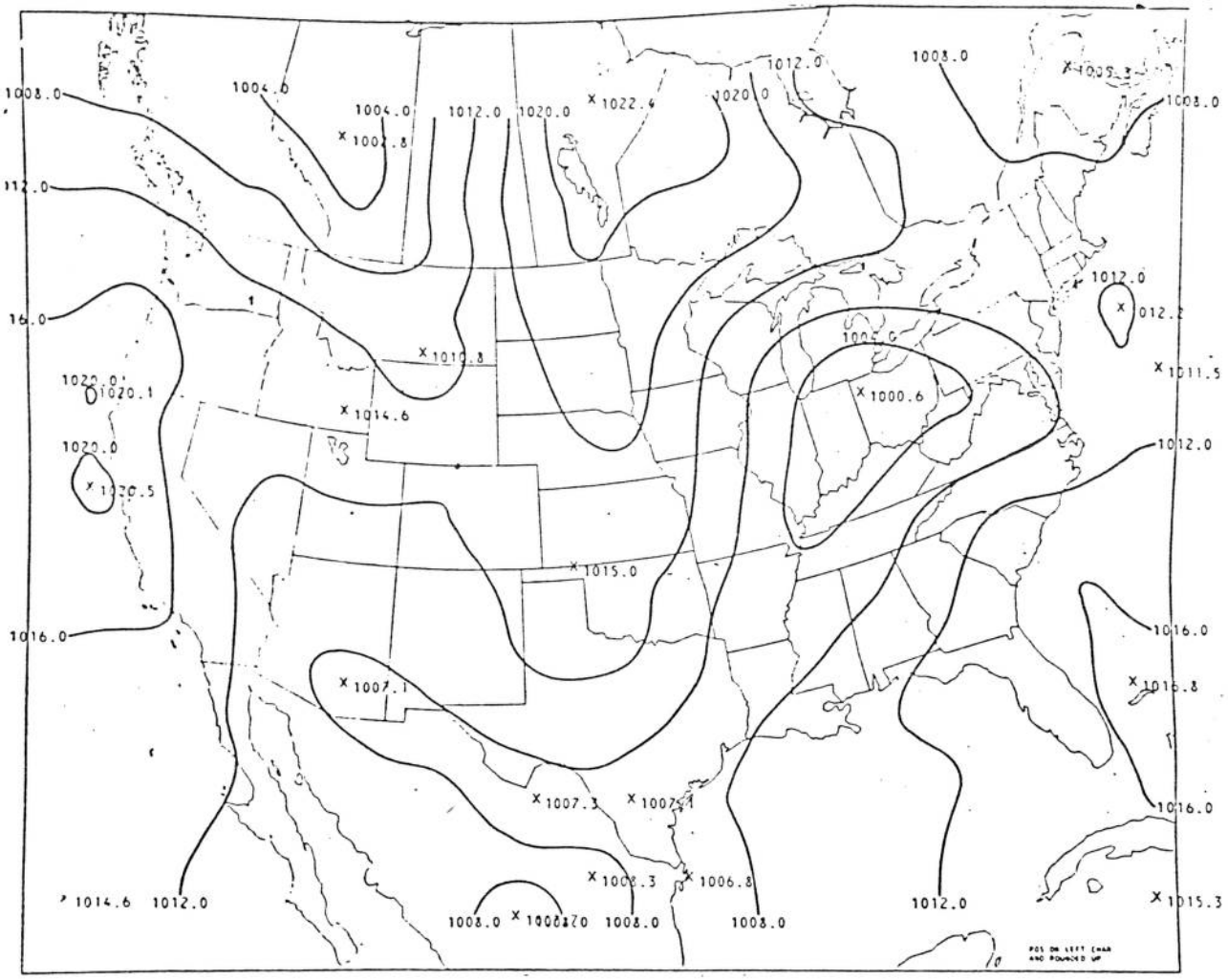

Figure 8a. Six-hour PCM SLP forecast valid 0300 GMT 9 April 1979.

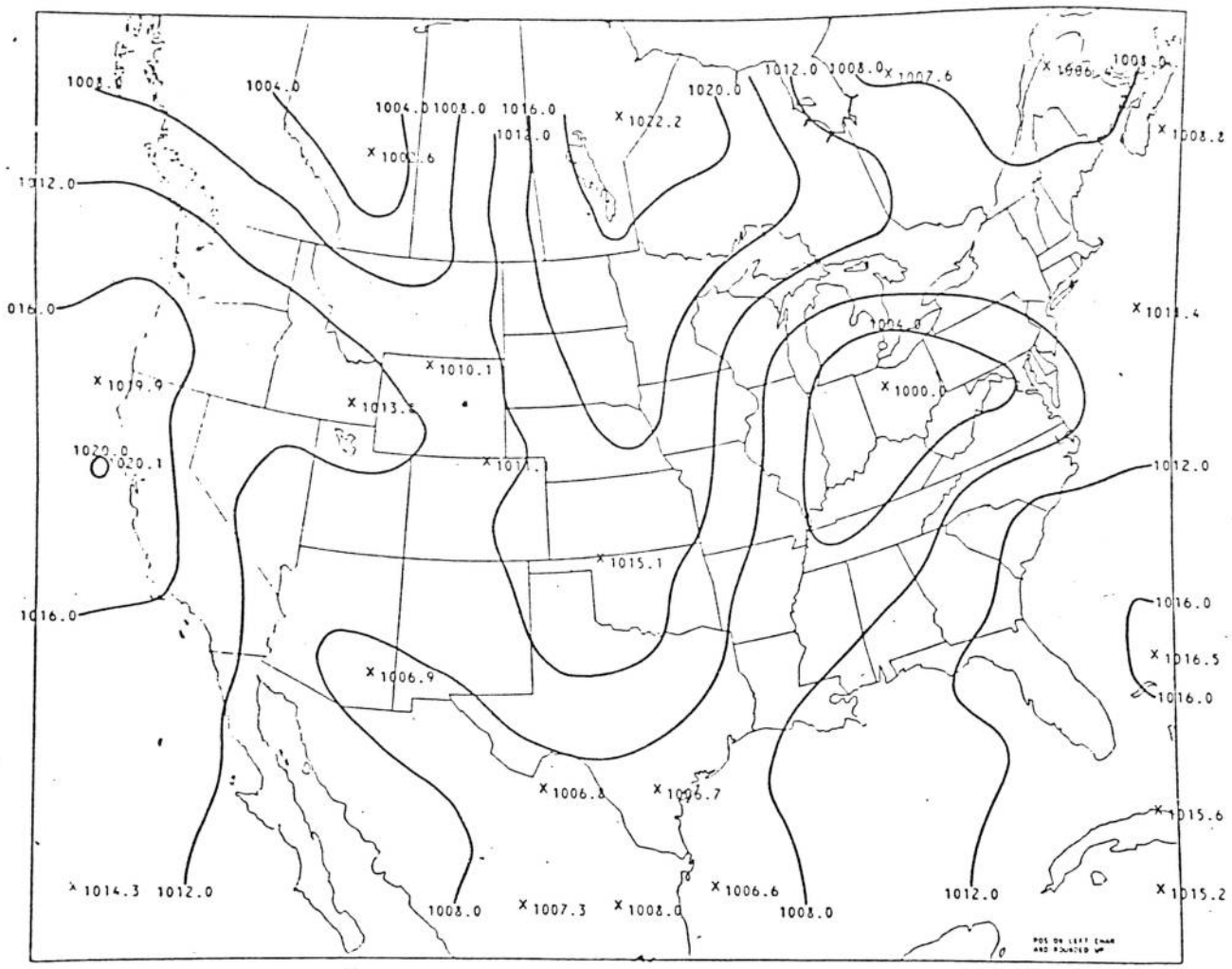

Figure 8b. Nine-hour PCM SLP forecast valid 0600 GMT 9 April 1979.

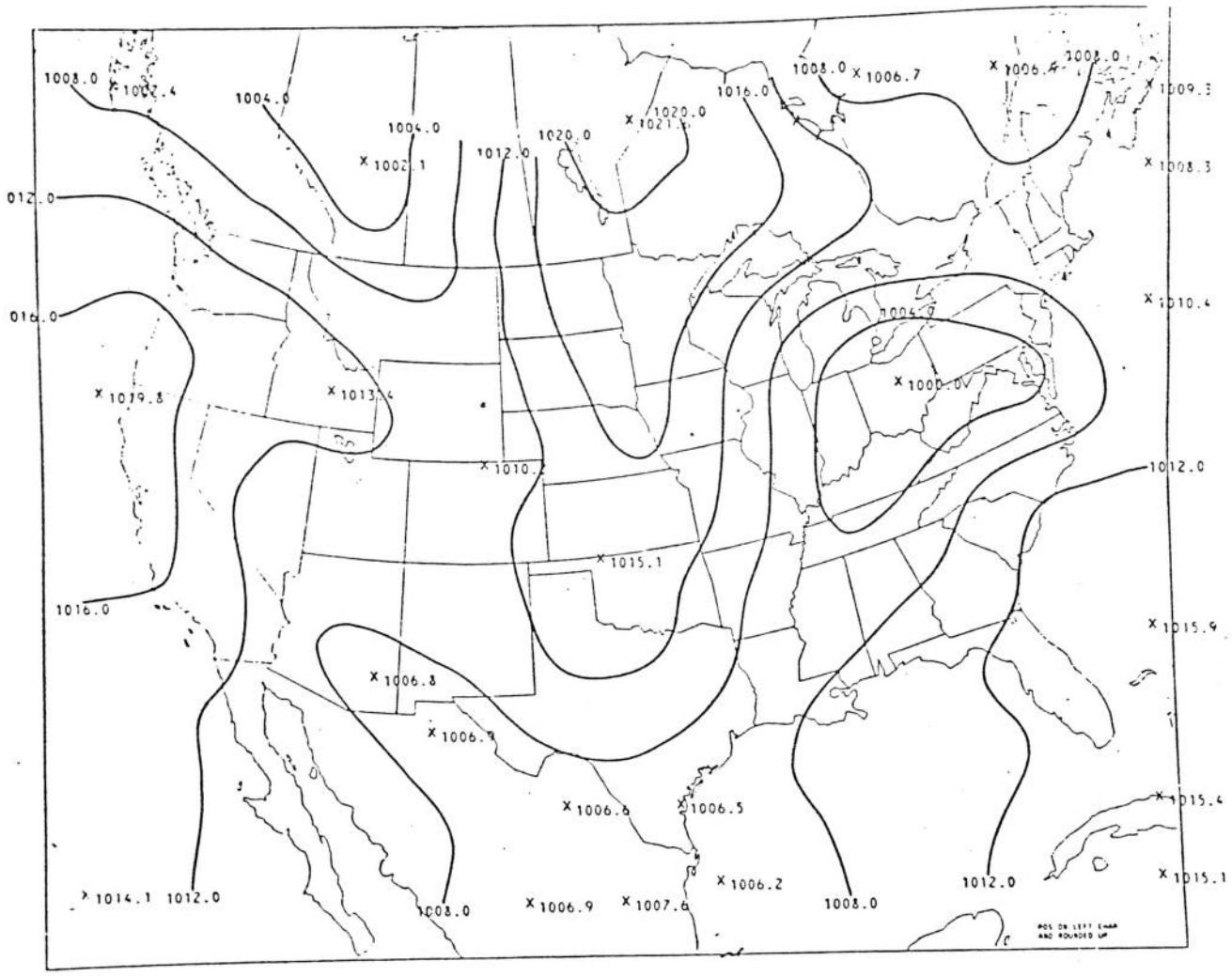

Figure 8c. Twelve-hour PCM SLP forecast valid 0900 GMT 9 April 1979.

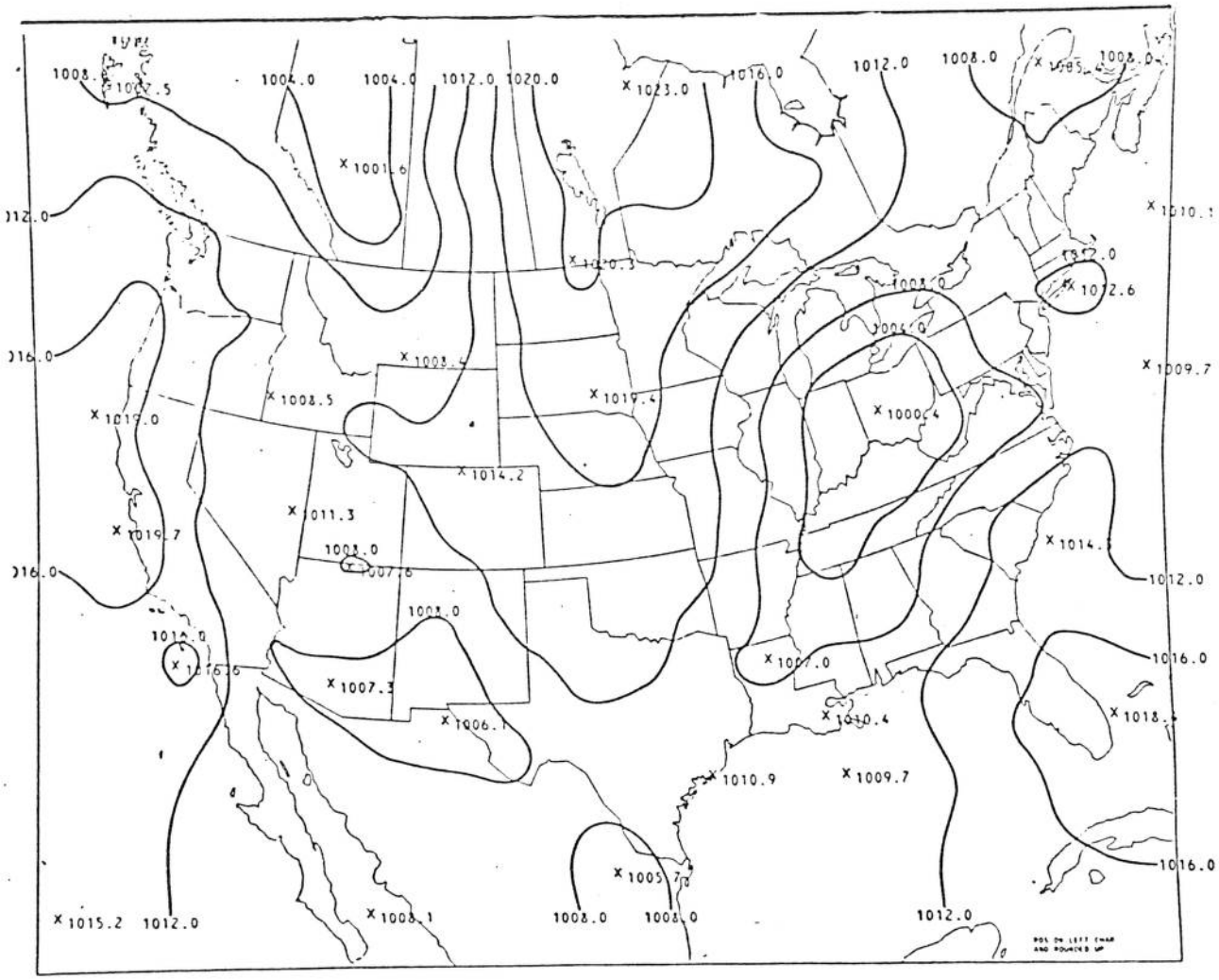

Figure 9a. SLP analysis valid 0300 GMT 9 April 1979.

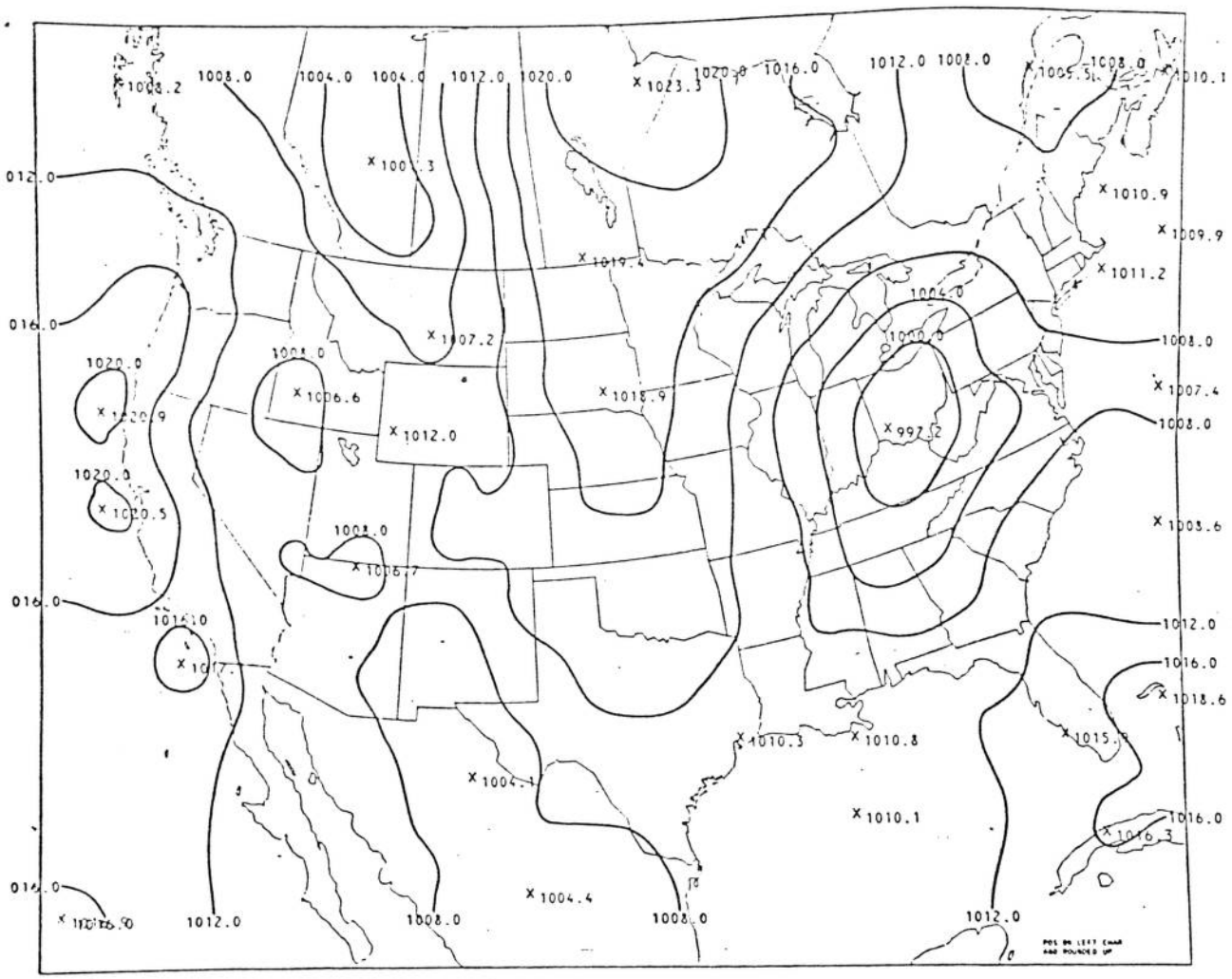

Figure 9b. SLP analysis valid 0600 GMT 9 April 1979.

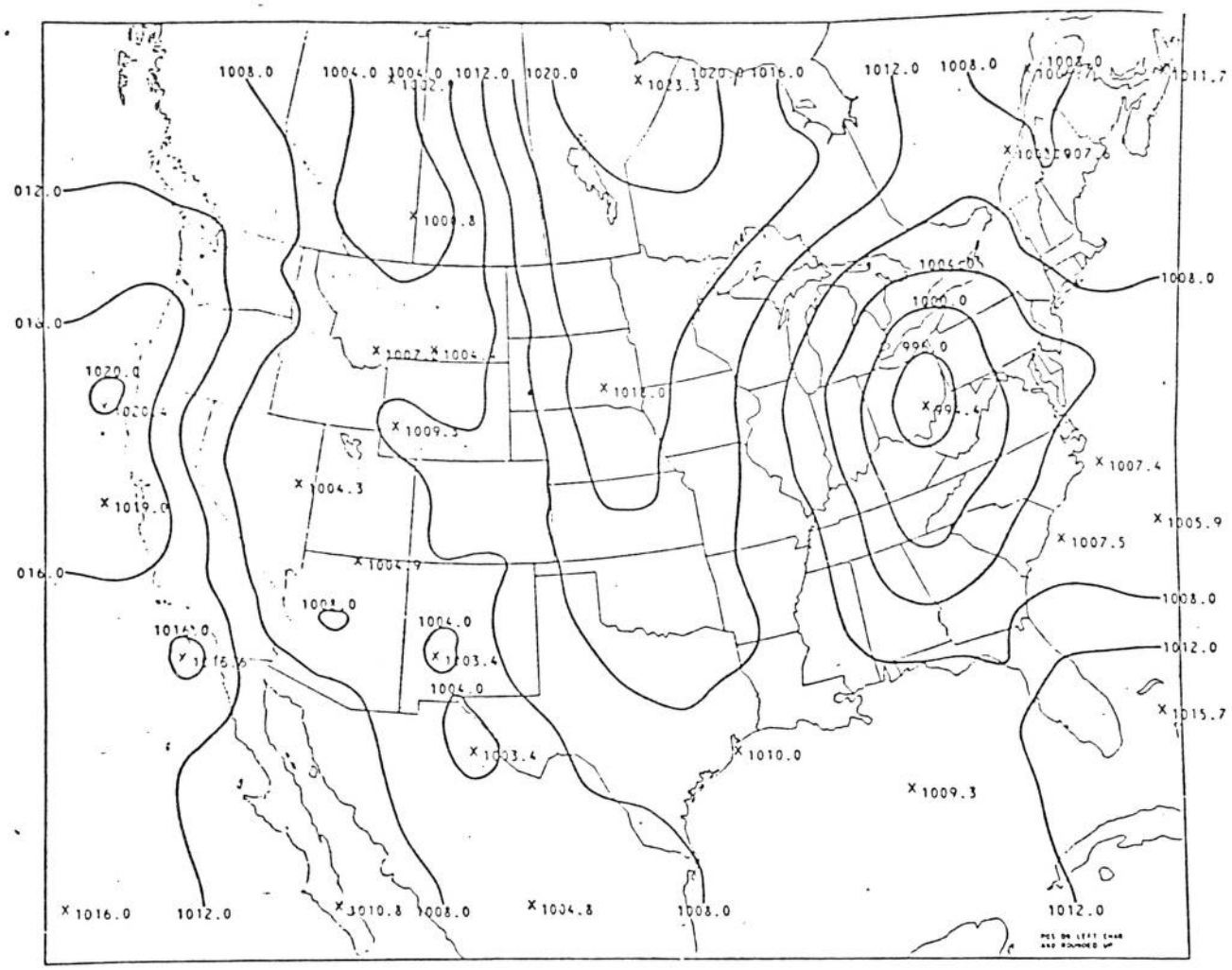

Figure 9c. SLP analysis valid 0900 GMT 9 April 1979.

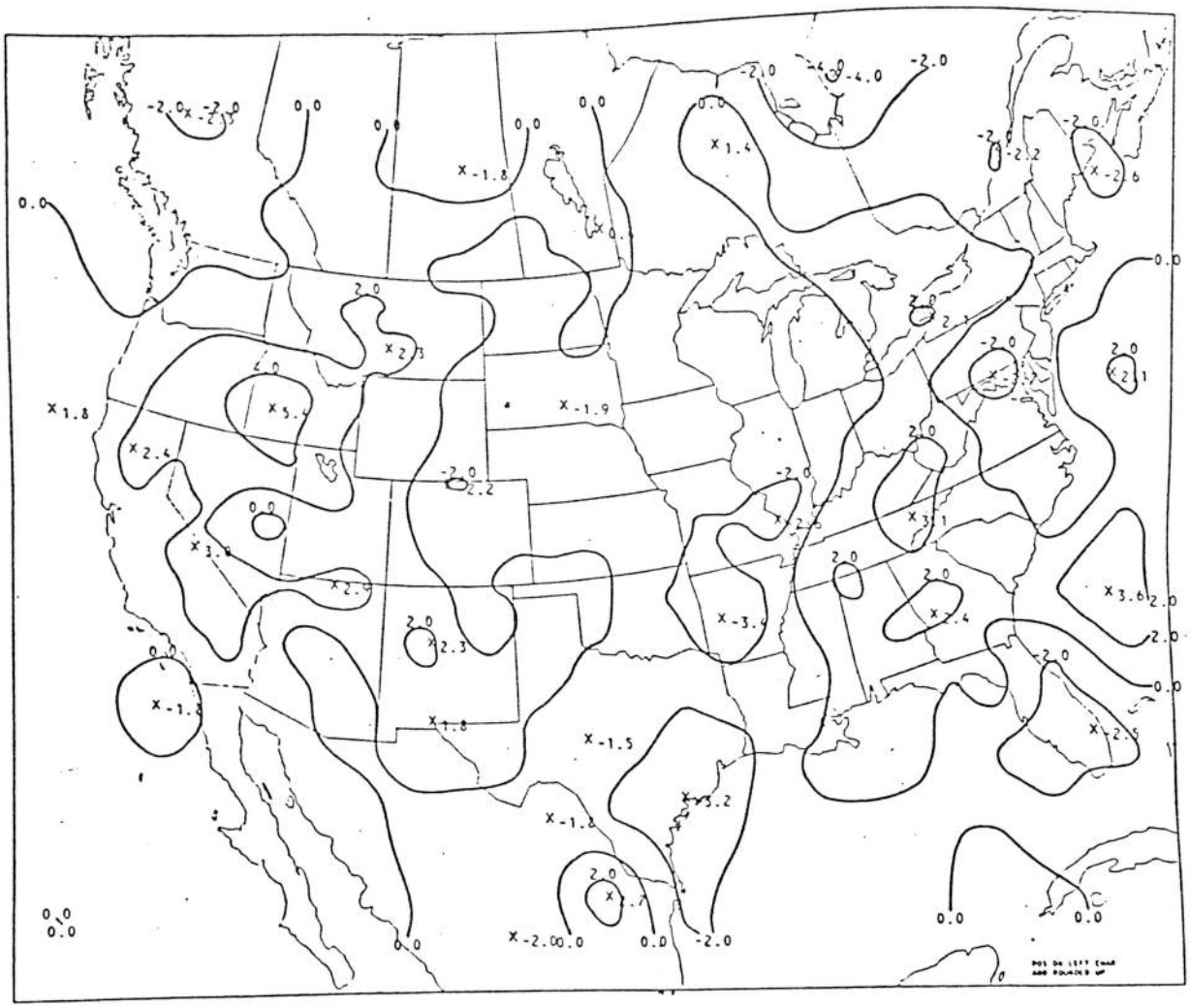

Figure 10a. Forecast error field (mb) corresponding to Fig. 8a.

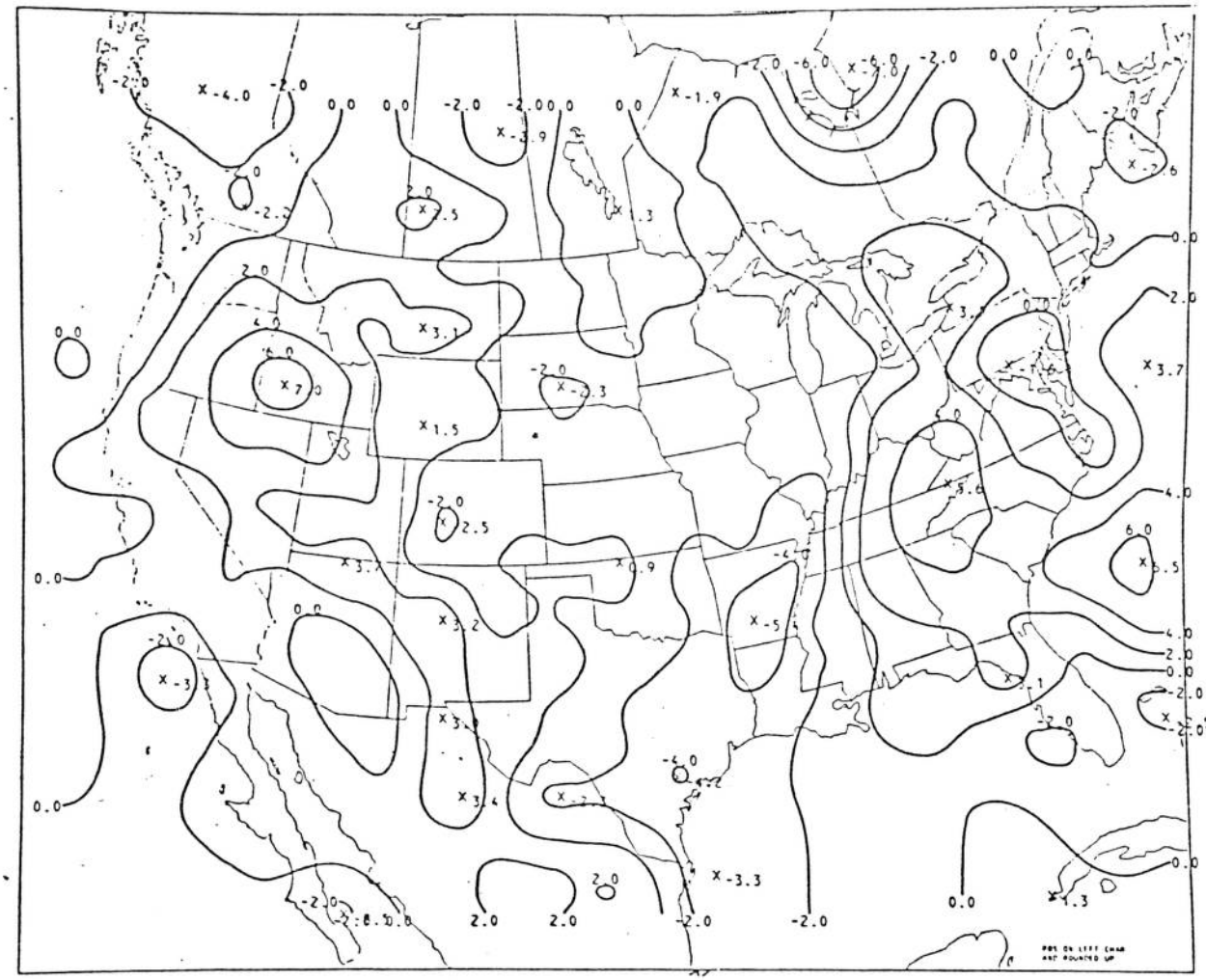

Figure 10b. Forecast error field (mb) corresponding to Fig. 8b.

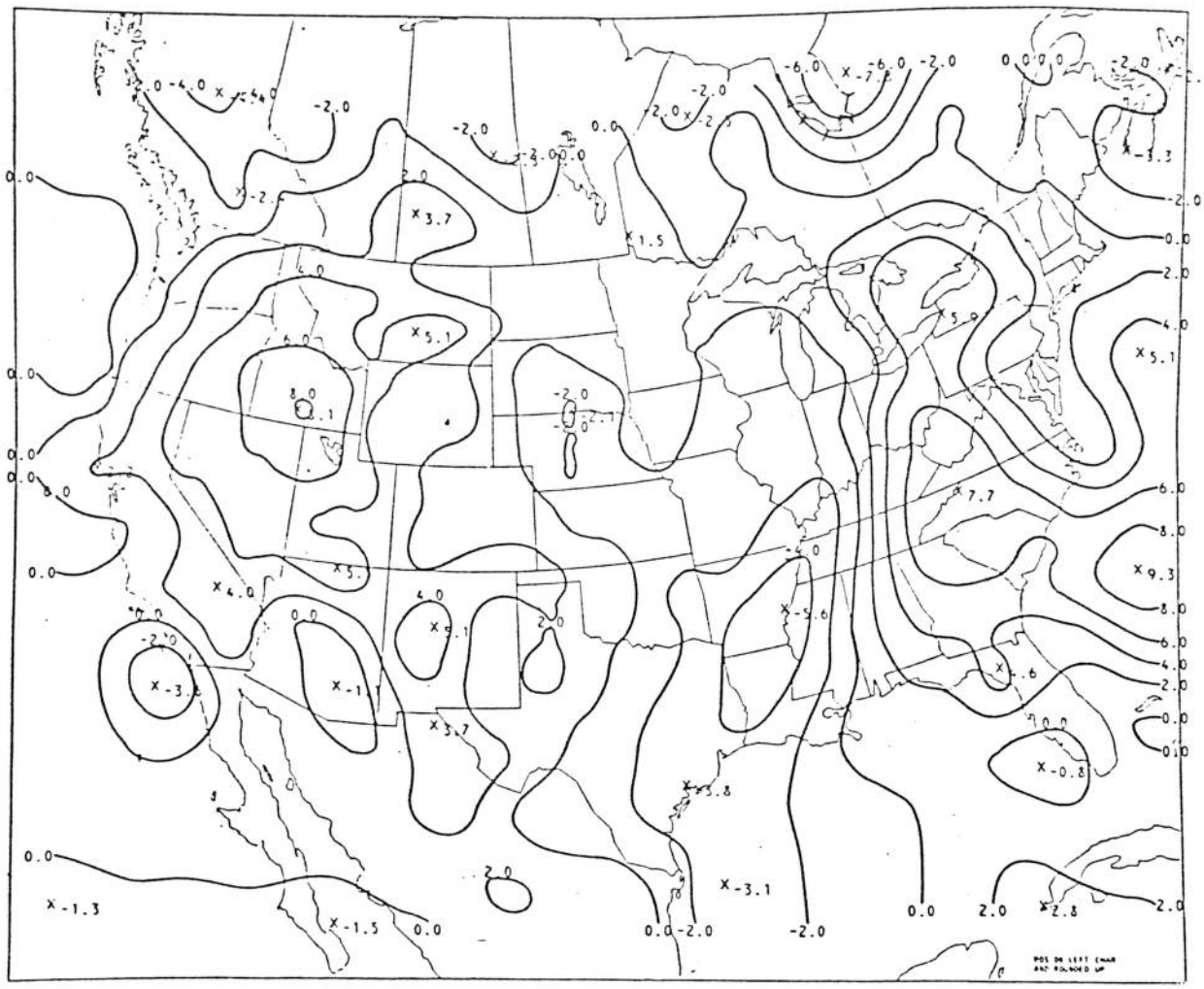

Figure 10c. Forecast error field (mb) corresponding to Fig. 8c.

APPENDIX A

MODIFICATION OF THE CRESSMAN OBJECTIVE ANALYSIS TECHNIQUE

The so-called Cressman (1959) analysis method for interpolating irregularly spaced data to a regular array of grid points is given by,

$$\hat{\phi}_{i+1} = \hat{O}_i + \frac{\sum_{k=1}^{N} w_k D_k}{\sum_{k=1}^{N} w_k}, \tag{4}$$

where, for a given grid point,

$\hat{\phi}_i$ = current analysis estimate of the scalar variable ϕ obtained on interpolation pass i,

$\hat{\phi}_{i+1}$ = the new analysis estimate obtained on pass (i+1),

D_k = difference between the current analysis and the observed value at station k,

N = number of observations within the circular influence region of radius R,

$w_k \left(= \frac{R^2 - d_k^2}{R^2 + d_k^2}\right)$ = the weight applied to D_k, and

d_k = distance between station k and the grid point of concern.

This interpolation method performs quite well when the data are rather uniformly distributed, but not so well when the data distribution is highly nonuniform. Note that, because of the division by the sum of the weights in Eq. (1), the weighting on an individual D_k depends only on the relative distances of the stations to the gridpoint, not on their actual distances. Also, no account is made for the directions of the stations from the gridpoint. This means that for a given set of D_k's, the analysis correction term, which is the second term on the right side of Eq. (4), could be the same for an assortment of station distributions as long as the relative distances in each set are the same. That is, the stations could be close, far away, and biased toward one direction from the gridpoint and the result could be the same. Thus, for our requirement of getting vector components on the 44x58 grid from the interior 2x3 or 7x10 arrays, the Cressman works well in the interior where the data coverage is uniform, but it works poorly near the borders of the grid where the data have to be extrapolated.

To improve the interpolation in nonuniform data coverage areas, Eq. (1) was modified to read,

$$\hat{\phi}_{i+1} = \hat{\phi}_i + f(d_c)\frac{\sum_{k=1}^{N} w_k D_k}{\sum_{k=1}^{N} w_k},$$

where,

$$f(d_c) = 1, \text{ for } d_c < C$$
$$= \cos \frac{\pi}{2}\left(\frac{d_c - C}{R - C}\right), \text{ for } C \leq d_c \leq R,$$

and d_c is the distance from the gridpoint to the centroid of the observations within the influence circle of radius R. C is a parameter that was assigned the value 0.45R, which is close to the moment of inertia of the circular area as weighted by the Cressman weight function (0.497R). The effect of $f(d_c)$ is to reduce the correction term in Eq. (5) when $d_c \geq C$ by effectively reducing the Cressman weight applied to D_k. The modified Cressman weight as a function of the normalized station distance for various values of d_c is illustrated in Fig. 11. Note that when the stations are rather uniformly distributed, d_c would be less than C and $f(d_c)$ would have no effect. Our experience with application of Eq. (2) is that the interpolated fields are the same as those obtained without the modification in the interior area of the grid, and substantially improved in areas where the data are extrapolated.

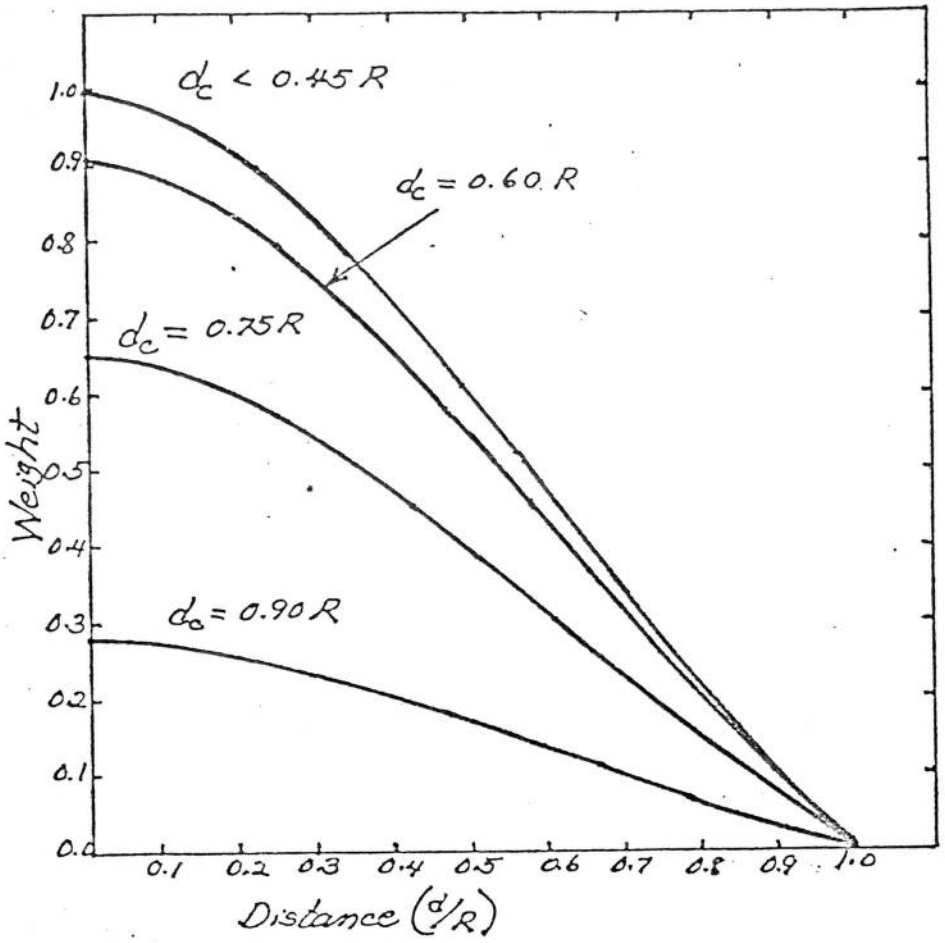

Figure 11. The modified Cressman weight function versus the normalized station distance, d/R, for various values of the centroid distance d_c. In the top curve, the Cressman weight function is not modified since $d_c < 0.45$ R.